Molecularly Imprinted Polymers (MIP) Combined with Raman Spectroscopy for Selective Detection of Δ⁹-tetrahydrocannabinol (THC)

by

Arian Yeganegi

B.Sc., Iran University of Science and Technology, 2020

A THESIS SUBMITTED IN PARTIAL FULFILLMENT OF

THE REQUIREMENTS FOR THE DEGREE OF

MASTER OF APPLIED SCIENCE

in

THE FACULTY OF GRADUATE STUDIES

(Department of Mechanical Engineering)

THE UNIVERSITY OF VICTORIA

July 2023

Supervisory Committee

Molecularly Imprinted Polymers (MIP) Combined with Raman Spectroscopy for Selective Detection of Δ⁹-tetrahydrocannabinol (THC)

Arian Yeganegi

B.Sc., Iran University of Science and Technology, 2020

Supervisory Committee:

Mina Hoorfar, Department of Mechanical Engineering
Supervisor

Mohsen Akbari, Department of Mechanical Engineering
Member

Karolina Valente, Department of Mechanical Engineering
Member

Abstract

This thesis presents the development of a proof-of-concept sensor for the sensitive and selective detection of Trans-Δ^9-tetrahydrocannabinol (THC) using a molecularly imprinted polymer (MIP) synthesized with a THC template. The sensor combines MIP technology with Raman spectroscopy to achieve label-free monitoring of THC based on a single identifying Raman peak. The MIP sensor exhibits a prominent peak at 1614 cm^{-1} in the Raman spectrum, attributed to the THC target molecule, enabling the selective quantification of bound THC with a low detection limit of 250 ppm. Comparative studies with a non-imprinted polymer (NIP) control demonstrate higher sensitivity of the MIP to the THC target molecule (67% higher average intensity), confirming the presence of THC-specific recognition sites within the synthesized MIP material. Additionally, the selectivity of the MIP-based sensor is demonstrated by analyzing the Raman spectrum of MIP exposed to Cannabidiol (CBD), ethanol, and acetone.

Keywords: Molecularly imprinted polymer (MIP), Raman spectroscopy, THC detection

Lay Summary

In this thesis a novel MIP-based sensor is developed for THC detection, utilizing Raman spectroscopy for label-free monitoring. The sensor demonstrates high sensitivity, selectivity, and a low detection limit for THC, offering potential applications in quality control, forensic analysis, medical diagnostics, and drug screening. The successful implementation of this sensor contributes to the advancement of THC detection technologies and provides a promising platform for the sensitive and selective quantification of THC in various analytical settings.

Preface

The research presented in this thesis is the original work performed by the author. This thesis was supervised by Dr. Mina Hoorfar at the Microfluidics and Nanotechnology (MiNa) laboratory in the Faculty of Mechanical Engineering at the University of Victoria.

Table of Contents

List of Tables

List of Figures

Acknowledgements

I would like to express my gratitude to Dr. Mina Hoorfar, my supervisor, Nishat Tasnim, our lab manager, and Somayeh Fardindoost, our postdoctoral fellow, for providing me with excellent support throughout this journey.

I am also immensely thankful to my amazing parents, lovely Negar, and precious friends, without whom I would not have been able to complete this endeavor.

Dedication

This thesis is dedicated to my beloved parents and Negar, who have supported me throughout my academic journey and provided me with unconditional love, encouragement, and inspiration. Their sacrifices and unwavering belief in me have made this achievement possible, and I cannot thank them enough for everything they have done for me.

I would also like to dedicate this thesis to my mentors at the University of Victoria, Dr. Mina Hoorfar, Dr. Somayeh Fardindoost, and Nishat Tasnim, whose guidance, expertise, and encouragement have been invaluable in shaping my research and academic growth.

Chapter 1: Introduction

1.1 Molecularly imprinted polymers (MIPs)

In this section molecularly imprinted polymers (MIPs), which are synthetic polymers that are designed to selectively recognize and bind to a target molecule [1], are discussed. In the beginning, a brief history and an introduction to this type of material is presented. Following, the application of MIPs in chemical sensing platforms is reviewed.

1.1.1 Introduction to MIPs

The idea of molecular imprinting has been around since the 1930s. The roots of the molecular imprinting concept can be traced back to when Soviet chemist Polyakov observed the remarkable adsorption properties of silica particles that were prepared in the presence of soluble additives. The basic principle of molecular imprinting, which involves creating a polymer network around a small template molecule to create a complementary nanocavity, was noted during this period [2], [3]. The first paper reporting on the development of MIPs, with the exact term “imprinted polymer” used, was published in 1984 by K. Mosbach and B. Sellergren in Lund, Sweden. G. Wulff also contributed to the development of MIPs and published papers on the topic in the 1980s. However, it was not until 1985 that Wulff used the term "imprinted polymer" to describe these materials. The difference between Mosbach and Sellergren's approach and Wulff's approach was that Mosbach and Sellergren focused on noncovalent interactions between the host and target, while Wulff tended to use covalent binding to create the imprint [3], [4].

In addition, the term "molecularly imprinted polymer sensor" was introduced by S. Piletsky in 1992, although the author had previously published papers on the production of MIPs in Russian literature as early as 1989. The development of MIPs has since led to research on various

applications of this technology, including separation and sensing materials, and catalytic reactions [4].

Molecularly imprinted polymers (MIPs) are synthetic materials that function like the biological antibody-antigen system by selectively binding to specific molecules. In other words, they are synthetic polymers that are designed to selectively recognize and bind to a target molecule. MIPs offer the same specificity and selectivity as biological receptors, but with added advantages such as durability and low cost [4], [5]. MIPs are fabricated in a variety of ways, but they all share a fundamental structure and are created using a process called molecular imprinting, which involves polymerizing a mixture of monomers, cross-linking agents, and a template molecule. Firstly, a polymer is created that includes the target or template molecule bound to a functional group of the host either covalently or noncovalently. Secondly, the template molecule is taken out from the polymer, leaving behind a specific cavity ready for rebinding. Finally, the MIP is exposed to a sample that contains the target molecule, and the cavity selectively takes up the target molecule from the complex sample [6], [7].

Due to their cross-linked nature, MIPs are resistant to harsh physical conditions, making them useful in various fields such as chemical separation, sensors, catalysis, and more. Another advantage of MIPs is their ability to be designed for almost any target molecule, regardless of size or complexity. Using MIPs with a sensing system can be useful for monitoring the environment or detecting abnormalities [2].

1.1.2 MIP Synthesis

In this section, the basics of the synthesis of MIPs are explained. MIPs are fabricated by imprinting synthetic copolymers with sites that are unique to a specific reference compound or a group of reference substances. These copolymers are highly cross-linked and act as a scaffold around the

template molecule or a dummy template molecule with a similar structure. This process results in the formation of a three-dimensional structure that captures and selectively binds the target molecule. In simpler terms, MIP materials are made by creating a mold of a specific molecule and using it to create a material that can selectively capture that molecule [8]. The key components needed for the proper synthesis of MIPs are the template molecule, functional monomer, cross-linking agent, reaction initiator, and solvent [9]–[11].

The shape and functionality of the cavities inside the MIP are defined through the template molecule. The choice of a template molecule (or its structural equivalent) is influenced by economic considerations, the availability of commercial sources, and the potential for establishing suitable interactions with different functional monomers. It is essential for the template molecule to possess chemical inertness and stability throughout the polymerization procedure [9].

The functional monomer is essential in the formation of a 3D polymer skeleton and is usually categorized into three common groups, acidic (for instance methacrylic acid and acrylic acid), alkaline (for instance 4-vinylpirydyne), and inert (for instance styrene) [9]. It should be noted that functional monomers play a crucial role in creating the binding sites within molecularly imprinted polymers (MIPs) and facilitating the binding interactions with target molecules [11].

The cross-linker in an imprinted polymer serves three main functions. Firstly, it controls the morphology of the polymer matrix. Secondly, it stabilizes the imprinted binding site. Lastly, it provides mechanical stability to the polymer matrix. Divinylbenzene (DVB), triethylene glycol dimethacrylate (TEGDMA), and ethylene glycol dimethacrylate (EGDMA) are widely used as common cross-linking agents in MIPs [9], [11].

The reaction initiator, which is typically used in small quantities (around 1% of the total weight of the reaction mixture), plays a crucial role in the formation of MIPs. This reaction component

belongs to the group of azo compounds and can generate free radicals when subjected to elevated temperatures or UV radiation. Common examples of reaction initiators include 1,1'-Azobis(cyclohexanecarbonitrile) (ACHN), 2,2'-Azobis(2-methylpropionitrile) (AIBN), and benzoyl peroxide [9].

The final major component is the solvent (progen) which has two essential functions. Firstly, it acts as a medium to bring together all the components involved in the polymerization, including the template, functional monomer(s), cross-linker, and initiator, into a single phase. Secondly, it plays a crucial role in creating the pores within polymers since it affects the conformations of polymer chains [9], [11].

The properties of synthesised MIPs such as their physical characteristics, structure, and effectiveness of them are affected by various factors such as the composition of the reaction mixture (including the selection of cross-linking monomer, functional monomer, and porogenic solvent), and the temperature and duration of the reaction. All these elements collectively influence the overall properties like morphology, and functionality of the MIP [10].

To create MIPs, a reaction mixture containing the key components explained above is prepared. During the polymerization process, a complex is formed between the template and the functional monomer. This complex is then surrounded by excess cross-linking monomer, resulting in the formation of a three-dimensional polymer network. Once the polymerization is complete, the template molecules are trapped within the polymer matrix. After that, thorough washing is carried out to remove the template molecules, leaving behind cavities that are complementary in size, shape, and molecular interactions to the original template molecule. This process is called molecular imprinting and the polymerization technique is called precipitation polymerization [10]. Precipitation polymerization is a technique used to produce MIPs by conducting cross-linking

polymerization in highly diluted monomer solutions that also contain the template species. In this process, the continuous phase of the reaction mixture becomes a nonsolvent for the formed polymer once it reaches a critical molecular weight. As a result, spherical MIP particles with diameters ranging from a few micrometers to smaller sizes are obtained [12]. MIP nanoparticles offer distinct advantages over other MIP types, including their greater surface-to-mass ratio, facilitating an increased number of accessible recognition sites. Additionally, MIP nanoparticles exhibit lower heterogeneities and improved solubilities, which have been pivotal in their effective utilization across a wide range of applications [3]. The fabrication process for MIPs is shown in Figure 1-1.

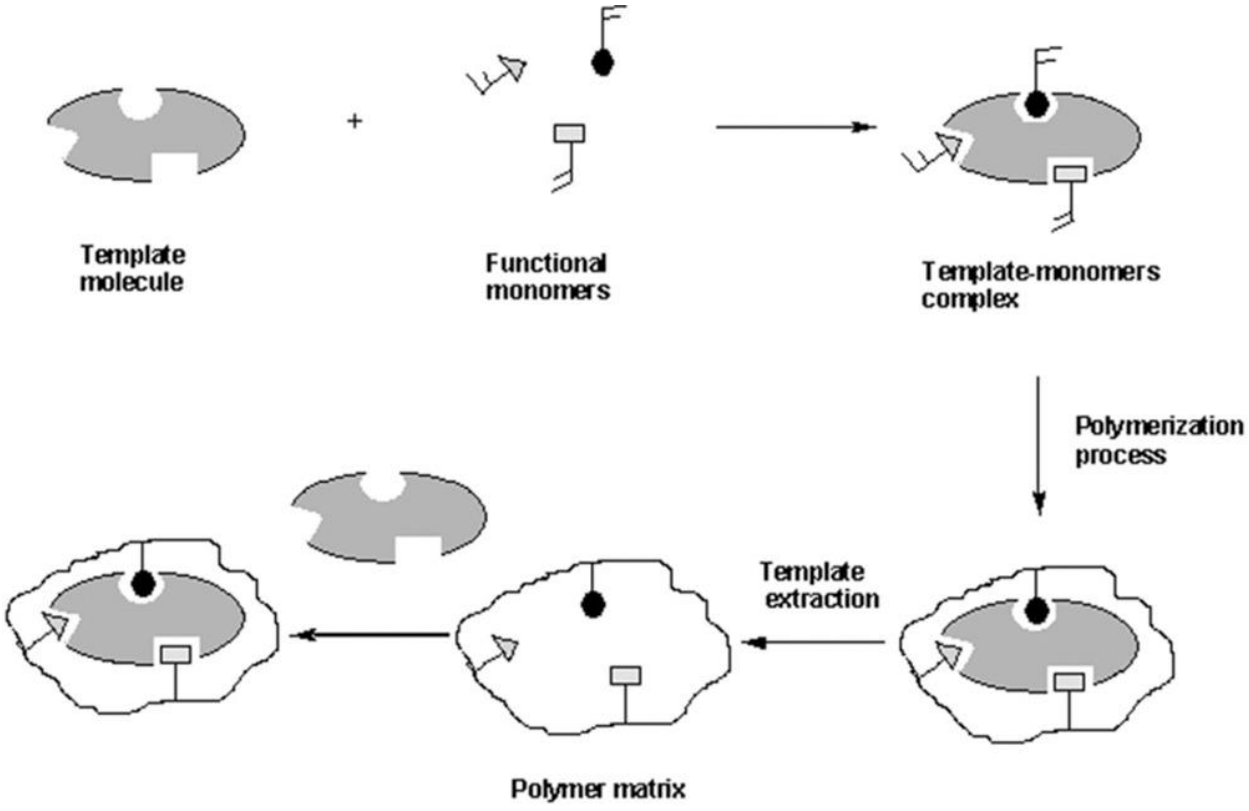

Figure 1-1. The synthesis process of MIPs [13].

1.1.3 Utilization of MIPs in sensing

MIPs have gained considerable interest as a highly promising material for sensing applications [14]. This is primarily due to their unique ability to possess selective binding sites that are specific to a variety target analytes. As it was briefly mentioned in section 1.1.2, during the synthesis of MIPs, functional monomers and crosslinking agents are polymerized in the presence of the template molecule as a mold, resulting in the formation of complementary binding sites in size, shape, and chemical functionality to the target molecule [2], [4], [6].

The history of usage of MIPs in sensing dates back to the 90s. For instance, Piletsky et al. developed a MIP-based sensor for the detection of low-weight organic molecules. In their paper, they highlight the advantages of MIP-based sensors, including stability, cost-effectiveness, and ease of fabrication. Furthermore, they point out to the fact that the ability to customize the molecular imprinting process enables the development of sensors with specific affinity towards different low-weight organic molecules [15]. On top of that, Mosbach provides insights into the preparation methods and analytical applications of MIPs, highlighting their importance in selective sensing and separation techniques. The paper also introduces the various fields of application for MIP-based sensors which include environmental monitoring, food safety, pharmaceutical analysis, and biomedical diagnostics [16].

MIP nanoparticles (NPs) have been used as the sensing layer in different traditional sensing platforms as they have significant advantages in their characteristics and properties. Their great features like improved chemical reactivity, binding capacity, and kinetics, as well as their uniform spherical shape, stability, and ease of dispersion, ease of preparation, reusability, and robustness for chemical and physical stresses have made them suitable candidates for integration with sensing platforms to produce MIP-based chemical sensors [6], [12].

One of the many applications of MIPs in sensing is selective sensing of different gaseous target analytes. In literature, MIPs have been combined with different transduction mechanisms to produce selective and sensitive gas sensors [6]. Some of the various approaches that were employed and combined with MIPs to detect and measure analytes are quartz crystal microbalances (QCM), electrochemical sensors , resistive methods, and optical sensors [2]. Here, some examples of utilization of MIPs for sensing is provided.

Zhang et al. investigated the gas-sensing properties of combination of single-walled carbon nanotubes (SWCNTs) and MIPs for methanol detection. The SWCNT-MIP composites showed enhanced sensitivity and selectivity compared to control samples. The results highlight the potential of these composites for developing efficient methanol gas sensors with applications in environmental monitoring and industrial safety [17]. In another study, Weng et al. presented a novel method for detecting gaseous formaldehyde. Their approach combined the sensitive mass detection capability of quartz crystal microbalance (QCM) with the exceptional selectivity and stability provided by MIPs. By leveraging these advantages, they achieved accurate and reliable determination of formaldehyde gas with a limit of detection of about 20.5 μM [18]. In another research, Haghdoust et al presented the development of a MIP-based QCM sensor for the selective detection of penicillins in aqueous media. The study focuses on designing MIPs with specific binding sites for three penicillins and immobilizing them on the QCM sensor surface. Through experiments and optimization, the sensor demonstrates high sensitivity, rapid response, and excellent selectivity towards penicillins, even in the presence of interfering substances [19]. Gaseous acetone was selectively detected, through resistive sensing, with a limit of detection of 66 ppm using a composite of MIPs and gold nanoparticles as the sensing layer by Jahangiri-Manesh et al. [20]. Volkle et al. developed a novel conductive MIP by blending of MIPs

with conductive polymers which resulted in a significant signal enhancement, both in QCM and resistive measurements, enabling the detection of R-(+)-limonene gas concentrations as low as 50 ppm [21]. In a recent study, Raziq et al. introduced the first-ever MIP-based electrochemical sensor for detecting the SARS-CoV-2 nucleoprotein (ncovNP). The sensor incorporates a disposable thin film electrode chip, equipped with MIP-based selectivity for ncovNP, and connected to a portable potentiostat. The resulting ncovNP sensor exhibited a linear response to ncovNP in lysis buffer, detecting concentrations as low as 15 fM and quantifying them down to 50 fM [22]. A sensor for direct detection of Hepatitis C Virus (HCV) using a MIP recognition element has been developed by Antipchik and colleuges. The integrated electrochemical sensor allows quantitative evaluation of HCV envelope protein E2 and HCV-mimetic particles in human plasma, with a low limit of detection of 4.6×10^{-4} ng/mL [23]. Feng et al. created a fluorescent sensor by combining a MIP layer with CdTe quantum dots (MIP-QDs) for detecting tetrabromobisphenol-A (TBBPA). The MIP-QDs composite showed desirable morphology and photoluminescence properties and the sensor exhibited a strong linear response in the concentration range of 1.0-60.0 ng/mL, with a low detection limit of 3.6 ng/g [24]. In another study, an optical sensor was developed using molecularly imprinted polymers coated with green carbon dots (CDs) for propranolol detection. The sensor exhibited a linear response in the concentration range of 0.8-65.0 nmol L−1 with a low detection limit of 0.2 nmol L−1. It demonstrated advantages such as cost-effectiveness, rapid response, high sensitivity, and selectivity for propranolol determination [25].

1.2 Overall background on cannabis

Cannabis, a plant belonging to the Cannabaceae family, has been widely cultivated and utilized for various purposes throughout history. It contains a diverse array of chemical compounds known as cannabinoids, which exhibit different properties and effects on the human body. This section

provides a comprehensive overview of cannabis, focusing on its two primary cannabinoids: Delta (9)-tetrahydrocannabinol (THC) and Cannabidiol (CBD) [26]–[28]. We delve into the chemical structures and physical properties associated with THC and CBD. Additionally, we explore the significance of THC detection. Furthermore, a review of THC detection techniques is presented to highlight the existing methodologies and advancements in the field. By gaining a deeper understanding of cannabis and its key constituents, we lay the foundation for the subsequent sections, where the combination of molecularly imprinted polymers (MIPs) and Raman spectroscopy will be investigated for THC sensing, providing a valuable contribution to the field of analytical chemistry.

1.2.1 Introduction to Delta (9)-tetrahydrocannabinol (THC) and Cannabidiol (CBD)

Delta (9)-tetrahydrocannabinol (THC) is the primary psychoactive compound found in cannabis plants. It is a member of the class of cannabinoids, which are a diverse group of chemical compounds naturally occurring in cannabis. THC is responsible for the euphoric and mind-altering effects commonly associated with cannabis use [28], [29].

The chemical formula of THC is $C_{21}H_{30}O_2$, the chemical structure shown in Figure 1-2, and it is is a lipophilic molecule, meaning it readily dissolves in fats and oils. It is a yellowish, sticky resin at room temperature and can also exist in crystalline form. The molecular weight of THC is approximately 314.46 g/mol. It exhibits a melting point range of 157-162 degrees Celsius [26], [28], [30].

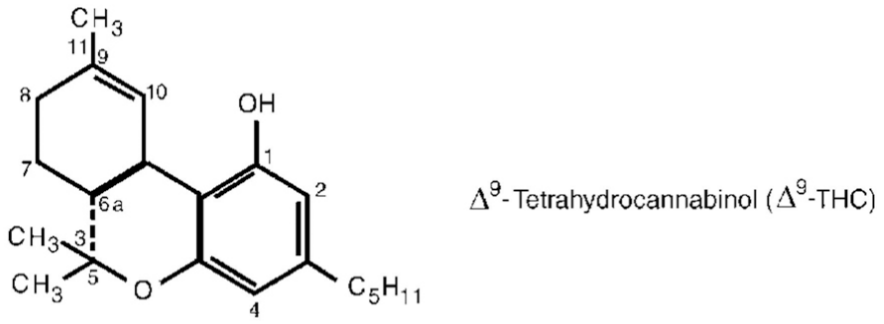

Figure 1-2. Chemical structure of delta (9)-tetrahydrocannabinol [26].

In addition to its psychoactive effects, THC has demonstrated various pharmacological properties. It interacts with the endocannabinoid system (ECS) in the human body, specifically binding to cannabinoid receptors. The CB1 receptors, predominantly found in the central nervous system, mediate the psychoactive effects of THC. Activation of the ECS by THC leads to the modulation of neurotransmitter release, resulting in altered cognitive and physiological responses [31], [32].

Beyond its recreational use, THC has been the focus of research due to its potential therapeutic applications. It has shown promise in the management of pain, nausea and vomiting, muscle spasms, and appetite stimulation. Furthermore, THC exhibits anti-inflammatory, neuroprotective, and antioxidant properties, making it of interest in various fields, including medicine and pharmacology [29], [33], [34].

Understanding the chemical and physical properties of THC is crucial for comprehending its interactions with the human body and its implications for health. Furthermore, investigating reliable detection techniques for THC is essential for ensuring accurate analysis and regulation in the cannabis industry.

Cannabidiol (CBD) is one of the major phytocannabinoids found in the cannabis plant, along with delta-9-tetrahydrocannabinol (THC). While THC is renowned for its psychoactive effects, CBD is non-intoxicating and does not induce the typical psychoactive effects commonly associated with

cannabis consumption. CBD has gained significant attention in recent years due to its potential therapeutic properties and its wide range of applications in the field of medicine [26], [35], [36]. Chemically, CBD is represented by the molecular formula $C_{21}H_{30}O_2$, the chemical structure shown in Figure 1-3, indicating its composition of 21 carbon atoms, 30 hydrogen atoms, and 2 oxygen atoms. It is a lipophilic compound, meaning it has a high affinity for fats and oils. CBD is typically derived from the industrial hemp plant, a variety of cannabis that has been selectively bred to contain high levels of CBD and negligible amounts of THC. The molecular weight of CBD is approximately 314.47 g/mol. It exhibits a melting point range of around 180 degrees Celsius [26], [30], [37].

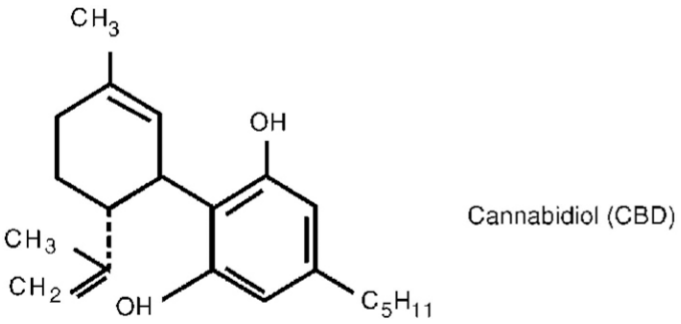

Figure 1-3. Chemical structure of CBD [26].

CBD is available in different forms, including oils, capsules, and edibles, catering to individuals seeking alternative remedies for their health and well-being. As research on CBD continues to expand, it holds the promise of offering novel treatment options for various medical conditions [35], [38].

By providing an overview of CBD's chemical composition, and non-intoxicating nature this section sets the stage for understanding the significance of CBD detection from THC, as they have a similar chemical structure.

1.2.2 THC sensing

The accurate detection of Δ^9-tetrahydrocannabinol (THC) is of great importance. The ability to reliably and selectively detect THC is crucial in various fields [39]. In this section, we will explore the significance of THC detection and review the existing techniques employed for its sensing. By understanding the importance of THC detection and examining the current methods available, we can appreciate the need for innovative approaches that offer improved sensitivity, selectivity, and convenience. The development of novel THC sensing techniques can contribute to advancements in various applications and ensure the safety and compliance of cannabis-related products.

1.2.2.1 Importance of THC detection

The detection of THC holds significance across various domains, including clinical, forensic, quality assessment, air quality monitoring, and law enforcement purposes. Firstly, understanding the impact of THC on the human organism and its medicinal benefits is crucial for medical practitioners and researchers. By detecting THC levels, medical professionals can gain insights into its effects and tailor treatment plans accordingly. Additionally, in the field of cannabis cultivation, the ability to determine different stages of plant growth through THC detection can aid growers in optimizing cultivation practices and ensuring desired potency [40].

Furthermore, for scientists in the laboratory, THC detection plays a vital role in quality assurance of cannabis products and provides valuable information for product development procedures. Moreover, in forensic analysis, the rapid detection of THC is essential for legal investigations, enabling accurate assessment of impairment levels and enforcement of cannabis-related driving regulations [40]–[42].

Finally, THC's intoxicating effects, including cognitive and motor function impairments, necessitate the development of simple, robust, and reliable detection techniques. This requirement

extends to various applications, ranging from clinical assessments to air quality monitoring, where the presence of THC needs to be identified accurately. Overall, the growing need for accurate THC detection is driven by cannabis legalization, common use, and the diverse applications that rely on its identification and quantification [43], [44].

1.2.2.2 Review of THC detection techniques

Various established techniques such as high-performance liquid chromatography (HPLC) and gas chromatography (GC) coupled with mass spectrometry (MS) or flame ionization detection (FID) are considered gold standards for THC determination [45]–[48]. However, these methods typically require sample pre-treatment and suffer from time-consuming and costly processing [49].

Mass spectrometry-based techniques, commonly used for THC analysis, provide high specificity and accuracy but involve complex and expensive processes. Sample transportation to a laboratory, followed by extractions, dilutions, incubations, centrifugations, and drying techniques, are necessary for THC detection in breath samples. Additionally, the standard THC detection method relies on blood samples, which require costly, intricate, and time-consuming chromatography with mass spectrometry analysis. These limitations have spurred scientists to develop portable, non-invasive, rapid, and cost-effective sensor technologies for on-site THC screening. The aim is to overcome the drawbacks of conventional methods and enable efficient THC detection in field and roadside testing scenarios [41]. Here, some examples of THC detection in literature is presented.

Mishra et al. have developed a wearable electrochemical sensor in the form of a ring for the simultaneous detection of THC in oral fluids. The sensor includes a voltammetric THC sensor and has a disposable sensing electrode ring cap for easy replacement. It utilizes multi-wall carbon nanotube/carbon electrode technology for THC detection. The sensor demonstrates fast and accurate detection of THC in diluted oral fluids without interference from the matrix. This portable

and convenient sensor shows potential for roadside drug testing and self-assessment by drivers prior to driving [50].

In a recent study, Ramzy et al. presented a review paper that focused on the innovative methods for the fast and precise detection of THC through breath analysis. In there they report that ongoing researchs are focused on exploring various techniques such as carbon nanotubes, biosensors, electrophoresis, and fluorescent probes as potential approaches for THC detection [41]. THC sensors were developed by Zhang et al. using carbon nanotubes (CNT) or carbon beads with poly(MAA-Co-EGDMA) through molecular imprinting technology. These sensors exhibited high sensitivity and selectivity for THC detection, surpassing nonimprinted polymer electrodes. The detection limit achieved by CNT-MIP electrodes was 0.18 ± 0.02 ng/mL. Morphological analysis confirmed the presence of polymers on the carbon material surfaces, and thermal stability was assessed through TGA [51]. In another study, Wanklyn et al. have developed a screen-printed carbon electrode sensor for the detection of THC in oral fluids. The sensor utilizes a reagent overlayer containing a mediator that reacts with THC to form an electrochemically active compound. The sensor demonstrated the ability to detect THC spiked in undiluted oral fluids within 30 seconds. However, the sensor's sensitivity was found to be lower than the acceptable criteria based on a trial with samples from cannabis smokers [52]. In a recent study, Solin et al. demonstrate the effective use of EDC/NHS coupling chemistry with nanocellulose to create efficient anchor layers for immobilizing anti-immune complex antibodies on surfaces. The unique properties of nanocellulose, including its high surface-to-volume ratio, abundance of OH groups, and hygroscopicity, facilitate surface functionalization and water permeation, providing a hydrophilic spacer for the sensing antibodies. THC detection is successfully achieved using both surface plasmon resonance (SPR) and paper-based sensing systems [53].

A category of previous research efforts have focused on the development of a portable Raman spectrometer, specifically designed for on-site applications, enabling the ultralow detection of THC in various sample matrices, including body fluids, plasma, and purified saliva. These studies have aimed to achieve exceptional sensitivity, allowing for THC detection at concentrations ranging from nano to picomolar levels. The utilization of Raman spectroscopy technology in these devices offers a non-invasive and rapid detection method, enabling efficient and reliable THC analysis in diverse real-world scenarios [54]–[56].

1.3 Raman spectroscopy based gas sensing technique

In this section, we delve into the application of Raman spectroscopy as a powerful technique for gas sensing. Raman spectroscopy has emerged as a valuable tool in various scientific and industrial fields due to its unique capabilities in molecular identification and characterization [57], [58]. In subsection 1.3.1, we provide an introduction to Raman spectroscopy, exploring its fundamental principles and highlighting its significance in analytical chemistry. Subsequently, in subsection 1.3.2, we delve deeper into the principles and advantages of utilizing Raman spectroscopy specifically for gas sensing applications. By understanding the underlying mechanisms and benefits of Raman spectroscopy in gas sensing, we can appreciate its potential for accurate and sensitive detection of gases in diverse environments.

1.3.1 Introduction to Raman spectroscopy

This section provides an introduction to Raman spectroscopy, explaining the underlying principles and techniques involved in the analysis of molecular vibrations. The basics of Raman scattering, instrumentation, and the interpretation of Raman spectra are discussed, setting the foundation for the subsequent discussion on its application in gas sensing.

Raman spectroscopy is an invaluable analytical technique that provides deep insights into the molecular composition and structural characteristics of various materials. It is based on the phenomenon of inelastic scattering of monochromatic light, typically from a laser source, by molecules within a sample. When light interacts with a sample and scatters, there are two outcomes: elastic scattering, known as Rayleigh scattering, and inelastic scattering, called Raman scattering. In elastic scattering, the scattered light retains the same energy as the incident light, resulting in the same frequency, wavelength, and color. In inelastic scattering, the scattered light has a different energy than the incident light, leading to a distinct frequency, wavelength, and color. This inelastic scattering process leads to a frequency shift in the scattered light, known as the Raman shift, which is directly correlated to the vibrational modes of the molecules. By analyzing the intensity and frequency of the scattered light, Raman spectroscopy enables the identification and characterization of chemical bonds, functional groups, and molecular interactions [59]–[61].

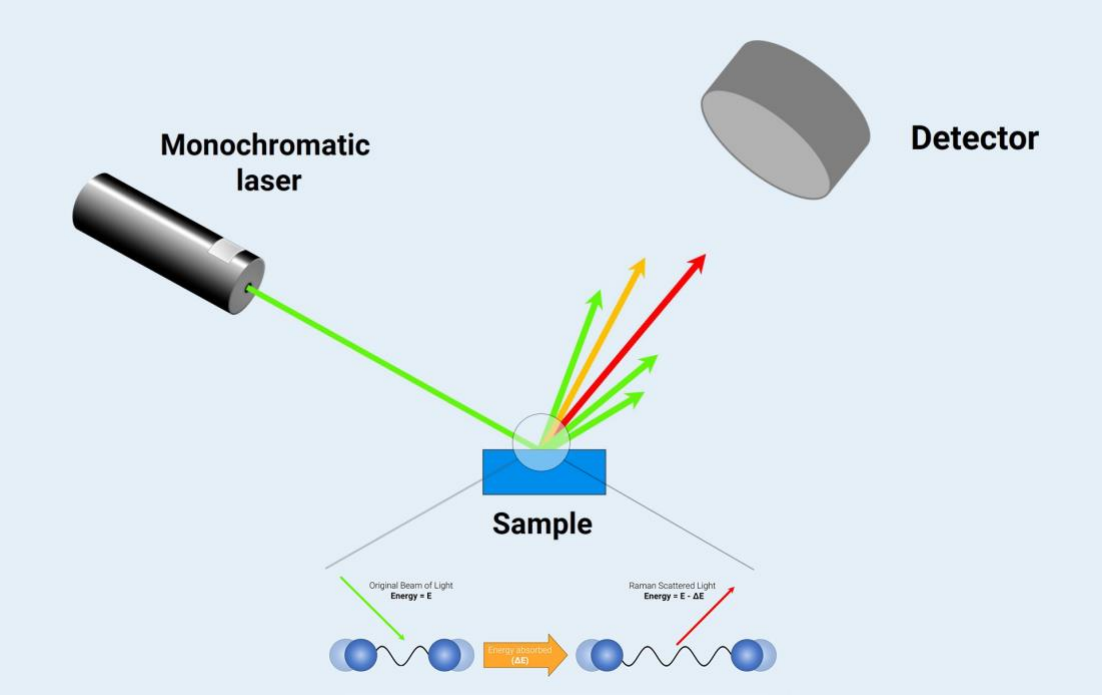

Figure 1-4. Basics of Raman spectroscopy [62].

The origins of Raman spectroscopy can be traced back to 1928 when Indian physicist Sir C.V. Raman discovered the Raman effect, for which he was awarded the Nobel Prize in Physics in 1930. Since then, Raman spectroscopy has evolved into a versatile and widely used technique in various scientific disciplines and industries [63].

The fundamental principle of Raman spectroscopy lies in its ability to provide detailed molecular information by probing the vibrational energy levels of molecules. When the incident laser light interacts with a sample, a small fraction of the scattered light experiences a change in energy due to molecular vibrations. This energy shift corresponds to the specific vibrational modes of the molecules, reflecting their unique chemical properties and structural arrangements. By analyzing the resulting Raman spectra, which consist of characteristic peaks at different Raman shifts, researchers can decipher the molecular fingerprint of the sample [59]–[61].

1.3.2 Principals and advantages of Raman spectroscopy in gas sensing

Here, the principles and advantages of Raman spectroscopy in gas sensing applications are elaborated. The unique features of Raman spectroscopy, such as its non-destructive nature, molecular specificity, and rapid analysis capability, are highlighted. Additionally, its ability to detect and identify various gases and volatile organic compounds (VOCs) makes it a promising technique for THC sensing.

Raman spectroscopy offers several unique advantages for gas sensing applications. One of the key principles of Raman spectroscopy in gas sensing is that each gas molecule has a specific Raman scattering fingerprint, which allows for the identification and quantification of different gases in a mixture. This enables selective and sensitive detection of gases with high specificity [64], [65].

One advantage of Raman spectroscopy in gas sensing is its non-destructive nature. It does not require sample preparation or direct contact with the gas, making it suitable for real-time

monitoring and remote sensing applications. Additionally, Raman spectroscopy is a label-free technique, meaning it does not require the use of additional chemical tags or probes for detection [66].

Raman spectroscopy also offers high sensitivity, especially when combined with advanced techniques such as surface-enhanced Raman scattering (SERS). SERS can enhance the Raman signal by several orders of magnitude, allowing for the detection of trace amounts of gases. This sensitivity, combined with the ability to detect multiple gases simultaneously, makes Raman spectroscopy a valuable tool for gas sensing in various fields, including environmental monitoring, industrial safety, and medical diagnostics [66], [67]. It must be noted that surface-enhanced Raman scattering (SERS) is a technique that enhances Raman signals by utilizing noble metals as SERS-active materials, enabling the detection of analytes at extremely low concentrations. This enhancement is achieved through the interaction between the incident laser and the noble metal nanoparticles or islands, which leads to the generation of intense localized electromagnetic fields known as localized surface plasmon resonances. These enhanced electromagnetic fields significantly amplify the Raman signals, allowing for highly sensitive detection and analysis of target analytes [68], [69].

Furthermore, Raman spectroscopy has a fast response time, enabling real-time monitoring and rapid detection of gases. It can provide qualitative and quantitative analysis, allowing for the determination of gas concentrations. The technique is also versatile and can be adapted for different gas sensing configurations, including fiber-optic probes for remote measurements and miniaturized handheld devices for on-site analysis [70]–[72].

Overall, Raman spectroscopy offers numerous advantages for gas sensing, including non-destructive analysis, high sensitivity, fast response time, and the potential for miniaturization and

portability. These features make it a valuable tool for a wide range of gas sensing applications, contributing to improved environmental monitoring, industrial safety, and health-related diagnostics.

1.4 Combination of MIP and Raman spectroscopy for sensing

This section explores the integration of molecularly imprinted polymers (MIPs) with Raman spectroscopy for sensing. Subsection 1.4.1 discusses the rationale behind combining MIPs and Raman spectroscopy, highlighting their unique advantages. Subsection 1.4.2 reviews previous studies on MIP-based Raman spectroscopy sensing, showcasing the potential of this combined approach for advanced sensing platforms.

1.4.1 Rationale for combining MIPs with Raman spectroscopy

Raman spectroscopy has emerged as a valuable technique for target analyte screening due to its non-destructive nature and high sensitivity. However, the presence of complex matrix interference poses a significant challenge in achieving accurate and reliable detection of target analytes. Complex matrices introduce background signals and interferences that can obscure the spectral features of the analytes, limiting the effectiveness of Raman spectroscopy as a standalone method. To overcome these limitations, researchers have recognized the potential of combining Raman spectroscopy with MIPs as a powerful approach for target analyte detection in complex matrices. By incorporating MIPs into the sensing system, the specificity of the detection process can be greatly enhanced [73].

The integration of MIPs with Raman spectroscopy offers several advantages. First, MIPs provide a selective recognition element that can effectively capture and bind the target analyte of interest, even in the presence of interfering substances within complex matrices. The tailored binding sites

in the MIPs ensure high affinity and selectivity towards the target analyte, enabling accurate detection and quantification [73], [74].

Second, Raman spectroscopy complements the MIPs by providing a sensitive analytical method for characterizing the molecular composition and vibrational characteristics of the analytes. The non-destructive nature of Raman spectroscopy allows for the direct analysis of samples without altering or destroying them. This enables the detection of target analytes in their native state, preserving their spectral signatures and facilitating reliable identification [66], [74].

1.4.2 Previous studies on MIP-based Raman spectroscopy sensing

In this subsection, we delve into previous studies that have explored the integration of MIPs with Raman spectroscopy for sensing applications, aiming to overcome the challenges posed by complex matrix interference.

The integration of MIPs with surface-enhanced Raman scattering/spectroscopy (SERS) has been widely explored as a potential method for chemical sensing in the fields of food safety, environmental monitoring, and clinical diagnostics. This approach involves combining MIPs, which are synthetic receptors with specific binding sites, with SERS, a technique that enhances Raman signals for improved detection sensitivity. By merging MIPs with SERS, researchers have developed chemical sensors that offer enhanced selectivity and sensitivity in detecting target substances [73].

Ren et al. conducted a study where they synthesized MIP-coated silver microspheres for the selective detection of bisphenol A (BPA) using SERS. The results demonstrated the high affinity and selectivity of the MIP-coated microspheres towards BPA, achieving a detection limit of 1 nM [74]. Lv et al. developed a selective molecularly imprinted plasmonic nanosensor capable of detecting protein biomarkers in human serum, with a limit of detection of 10 nM [75]. Similarly,

Bompart et al. synthesized composite MIP particles containing SERS-active silver nanoparticles and selective binding sites for (S)-propranolol, resulting in a sensitive nanosensor with a detection limit of 100 nM [76]. Araki et al. developed a sandwich-structured SERS substrate comprising an organic layer positioned between an Au thin layer and a layer of gold nanoparticles (AuNPs). Notably, the organic layer was molecularly imprinted to enable selective gas detection. Raman spectra obtained using the MIP-SERS substrate exhibited distinct peaks corresponding to the target gas molecule, 2-phenylethanol [77].

In another study, a selective and sensitive MIP-based SERS sensor was developed for detecting paclobutrazol residues in complex environments. By optimizing the SERS substrate and utilizing MIPs, the sensor achieves a detection limit of 0.075 μg/g in soil [78]. Ekmen et al. proposed a MIP-SERS sensor for quantifying malachite green (MG) in tap water and carp samples. Magnetic nanoparticles with molecular imprints (MIP@Fe3O4 NPs) are synthesized using reversible chain transfer catalyzed polymerization (RTCP). The MIP@Fe3O4 NPs exhibit high selectivity and adsorption capacity. A silver dendrite-based SERS platform is used for analysis, achieving low detection limits [79].

These examples highlight the potential of combining MIPs with Raman spectroscopy to create highly selective and sensitive sensors for various target analytes in different sample matrices. These sensors find applications in areas such as food safety, environmental monitoring, and clinical diagnostics. Some of these sensor technologies have been reviewed by Ma et al. [73].

1.5 Motivation and objective

This section presents the motivation behind the current study and defines the specific objectives that the research aims to achieve. It discusses the significance of developing a selective and

sensitive THC detection method based on MIPs and Raman spectroscopy, highlighting the potential impact and applications of such a system.

The detection of THC, the main psychoactive compound in cannabis, holds significant importance due to its widespread use and potential implications in various fields. The objective of this thesis is to combine MIP and Raman spectroscopy to develop a sensor that enables selective detection of THC. The motivation behind this research lies in the need for sensitive and selective THC detection methods that are fast, non-invasive, and can be applied in diverse settings. By achieving these goals, this study aims to contribute to the advancement of THC detection technologies for applications in areas such as quality control, forensic analysis, medical diagnostics, and drug screening.

1.6 Thesis Outline

The synthesis of MIP and NIP NPs, characterization methods, sensor preparation and gas sensing setup are presented in Chapter 2:. Next, the results obtained from characterization and gas sensing are shown in Chapter 3:. In the end, a brief review of the achievements and contributions and future works are presented in Chapter 4:.

Chapter 2: Methodology

2.1 Materials

In this section, a list of the main materials used in this study and where they were obtained from is presented. These materials were crucial in conducting the experiments and synthesis conducted throughout the study, and their selection was based on their properties and suitability for the intended purposes.

The following substances were procured from Sigma-Aldrich: Methacrylic acid (99%), Ethylene glycol dimethacrylate (98%), Acetonitrile, 2,2′-Azobis(2-methylpropionitrile), Acetone, and Ethanol.The rest of the materials used in this study are low temp Bath oil purchased from VWR, Δ^9-tetrahydrocannabinol (THC) acquired from Superior Extracts, and Cannabidiol (CBD) obtained from Honest Botanicals.

2.2 MIP and NIP NanoParticles synthesis

This section provides detailed method of MIP and NIP NPs fabrication. The precipitation polymerization method was employed to synthesize MIP nanoparticles in this study. The detailed procedure involved the following steps as shown in Figure 2-1 and Figure 2-2:

1. Firstly, 253 microliters of methacrylic acid (MAA) were combined with 30 milliliters of acetonitrile, which served as the functional monomer and solvent respectively in the synthesis process. This mixture ensured the presence of the necessary building blocks for the polymerization.

2. Subsequently, 314 mg of Δ^9-tetrahydrocannabinol (THC) distillate, a specific compound acting as the template molecule, was added to the MAA-Acetonitrile mixture. The addition of the template molecule was followed by 20 minutes of magnetic stirring to ensure a homogeneous distribution within the mixture.

3. To facilitate the formation of a crosslinked polymer network, 566 microliters of ethylene glycol dimethacrylate (EGDMA), functioning as the crosslinker, was introduced to the mixture. Additionally, 80 mg of 2,2′-Azobis(2-methylpropionitrile) (AIBN), serving as the initiator, was added. Magnetic stirring was continued for 2 minutes after the addition of EGDMA and AIBN.

4. To prevent light exposure, the glassware containing the mixture was covered with aluminum foil. Nitrogen gas was then purged into the mixture for 15 minutes to create an inert atmosphere. This is done to prevent the presence of oxygen, which can interfere with the polymerization process.

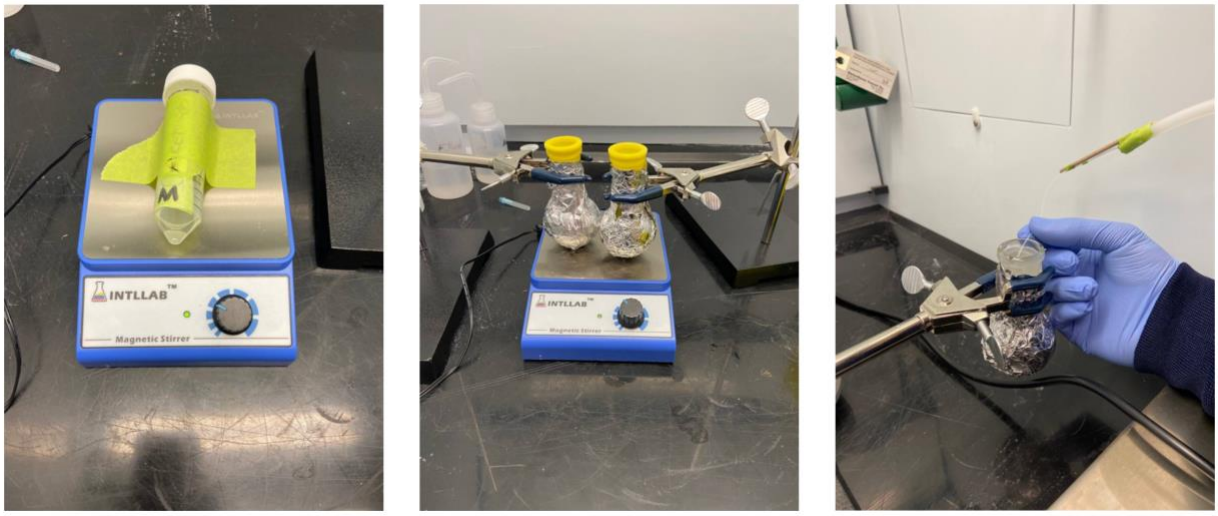

Figure 2-1. Synthesis process steps 1 to 4: (a) Mixing using a magnetic stirrer (steps 1 and 2), (b) Mixing and using aluminum foil for light exposure prevention (steps 3 and 4), (c) Purging nitrogen gas (step 4).

5. The mixture was transferred to an oil bath and subjected to a temperature of 60 ℃ for a duration of 14 hours. This allowed for the polymerization reaction to take place, resulting in the formation of MIP nanoparticles.

6. After completion of the polymerization process, the next step involved the removal of the template molecule. The mixture was subjected to a sonicator for 5 minutes, followed by 5 minutes

of magnetic stirring. This sonication-stirring cycle was repeated 4 to 5 times to ensure efficient removal of the template.

7. In order to separate the synthesized nanoparticles, the magnets within the glassware were removed, and the mixture was centrifuged for 10 minutes at a speed of 6000 rpm. This centrifugation step helped in the separation of the nanoparticles from the remaining solution. The process of centrifugation and nanoparticle separation was repeated seven times to ensure thorough template removal.

8. Finally, the synthesis of the non-imprinted polymer (NIP) was carried out using the same procedure as mentioned above, but with the omission of the step involving the addition of THC (template). This allowed for the fabrication of control nanoparticles without the presence of a specific template molecule.

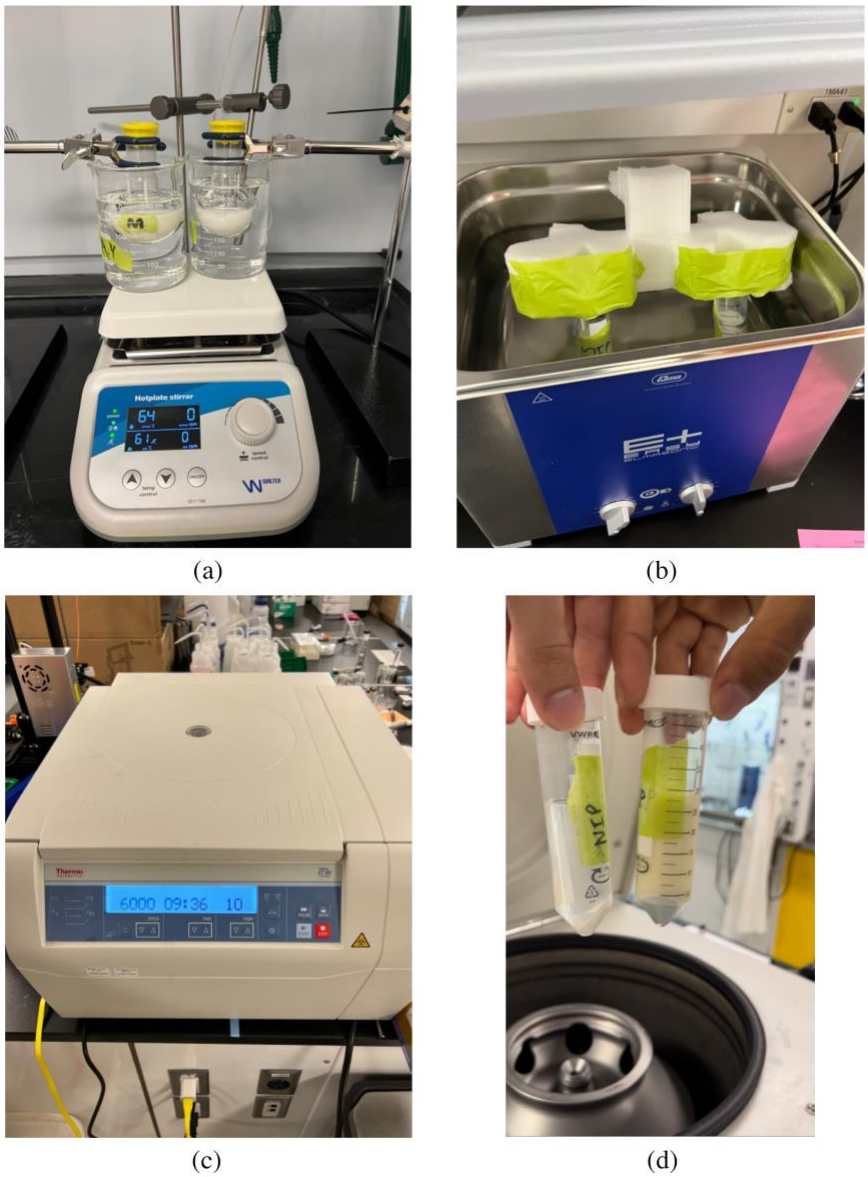

Figure 2-2. Synthesis process steps 5 to 8: (a) Polymerization in the oil bath (step 5), (b) Sonication for template removal (step 6), (c,d) Sonication for MIP and NIP NPs separation (steps 7 and 8).

By following this detailed procedure, MIP nanoparticles were successfully synthesized, while NIP nanoparticles were synthesized as a control group for comparison purposes. Figure 2-3 shows the schematic of MIP NPs synthesis used in this research.

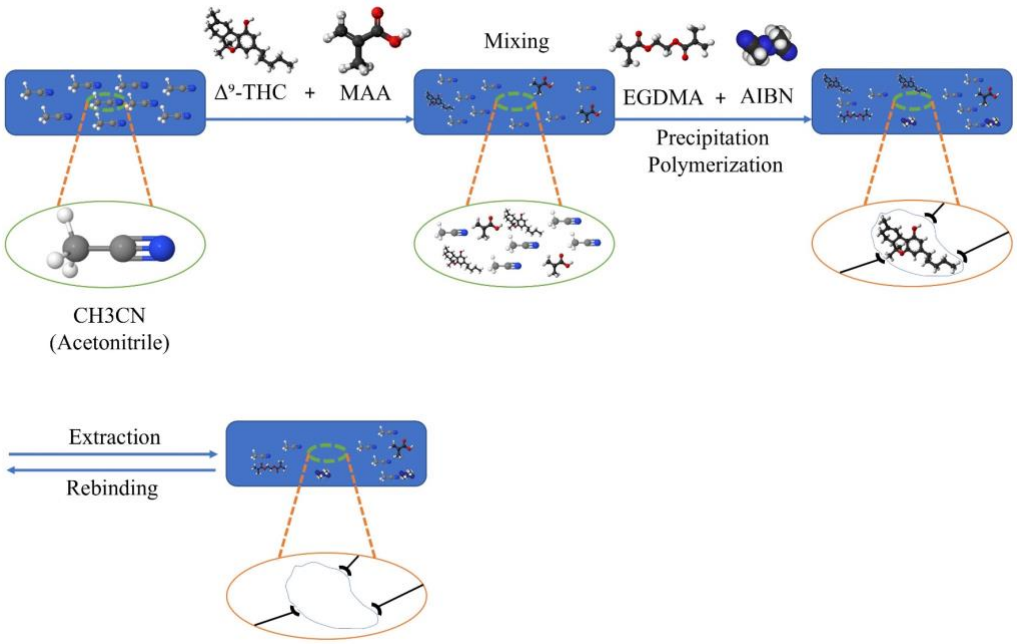

Figure 2-3. Schematic of MIP NPs synthesis.

After the synthesis of the nanoparticles, characterization tests were conducted to understand the morphology, size distribution and chemical composition and other properties of the synthesized material.

2.3 MIP and NIP NanoPatricles characterization

In this thesis, Raman spectroscopy and scanning electron microscopy (SEM) are used to characterise synthesised MIP and NIP nanoparticles. The morphology and structural aspects of the nanoparticles are investigated using these characterization techniques, which offer important information about their physical properties and molecular interactions. High-resolution imaging provided by SEM makes it possible to see the size, shape, and surface morphology of the particles [80], [81]. On the other hand, Raman spectroscopy offers comprehensive details about the molecular structure and chemical composition of the synthesised nanoparticles [82], [83]. It is possible to gain a thorough understanding of MIP and NIP nanoparticles by using these complimentary methodologies.

2.3.1 Scanning electron microscopy (SEM)

Scanning electron microscope is an instrument used to visualize surface topography and gather material information from conductive specimens. It operates by directing a focused beam of high-energy electrons onto the specimen, which is then deflected by a magnetic field and scanned in a raster pattern to capture the surface details. During imaging, interactions between the electron beam and the specimen are detected and converted into grey values. Nonconductive surfaces need to be coated with a conductive layer to enable imaging in the SEM [80], [81].

In the characterization of the synthesized MIP and NIP nanoparticles, scanning electron microscopy was done using a Hitachi SEM electron microscope. For sample preparation, MIP and NIP NPs were coated on a glass substrate by dropcasting. Since, MIP and NIP NPs are nonconductive, gold sputter coating was done on the samples before SEM was conducted.

The examination of the MIP and NIP particles' size and shape was performed using the Hitachi S-4800 SEM instrument, within the Advanced Microscopy Facility at the University of Victoria. For imaging, the accelerating voltage was set to 1 kV, and two working distances of 4 mm and 8 mm was used. Subsequently, the acquired SEM images were used to analyze the morphology and size distribution of the particles, using ImageJ software.

2.3.2 Raman spectroscopy

For chemical composition characterization of the synthesized MIP and NIP nanoparticles Raman spectroscopy was conducted, which offers valuable insights into their chemical bonds and molecular structure. Raman spectroscopy is a non-destructive technique based on the interaction of light with the vibrational modes of molecules. By irradiating the nanoparticles with a laser, Raman scattering occurs, resulting in a spectrum of scattered light that can be analyzed to identify and quantify the molecular components present in the samples [82], [83].

In this study, a high-resolution Raman spectrometer (Renishaw inVia Raman system) was employed to collect the Raman spectra of the MIP, NIP, and MIP before template removal nanoparticles. The laser excitation wavelength used was 532 nm, which ensures optimal interaction with the nanoparticles. The Raman spectra were recorded over a range of 100−3200 cm^{-1}, allowing for the detection of characteristic vibrational bands associated with the functional groups and molecular structures of the nanoparticles. Subsequent analysis of the obtained Raman spectra provides crucial information about the presence of specific chemical bonds, confirming the successful synthesis of MIP and NIP nanoparticles and enabling a deeper understanding of their structural properties.

2.4 Sensing layer preparation

For conducting Raman spectroscopy with minimal background noise, a Ø1" Protected Silver Mirror from Thorlabs was selected as the sensing substrate. This choice ensured a low level of interference and allowed for accurate sensing using the MIP nanoparticles. To prepare the samples for analysis, the fabricated MIP nanoparticles were dispersed in acetonitrile using ultrasonication for 5 minutes, followed by further mixing using a vortexer for 1 minute.

The surface of the sensing substrate was meticulously prepared to ensure optimal adhesion and uniformity of the nanoparticle dispersion. It involved washing the substrate with 70% ethanol to remove any contaminants and subsequently allowing it to air dry. Once the substrate was prepared, 10 microliters of the thoroughly dispersed MIP and acetonitrile mixture, with a concentration of 2.84 mg/ml, were drop-casted onto the sensing substrate. Similarly, for the NIP exposure, the same procedure was followed, where 10 microliters of the thoroughly dispersed NIP and acetonitrile mixture, also with a concentration of 2.84 mg/ml, were drop-casted onto the sensing substrate. The drop-casted sample was then left to dry for an hour under a fume hood, facilitating the evaporation

of the solvent and the formation of a uniform nanoparticle layer on the substrate surface. This preparation method ensured consistent and reliable Raman spectroscopic measurements of the samples while minimizing any potential interference from the background. Figure 2-4 (a,b) depicts the substrate after the washing process and after dropcast of MIP mixture.

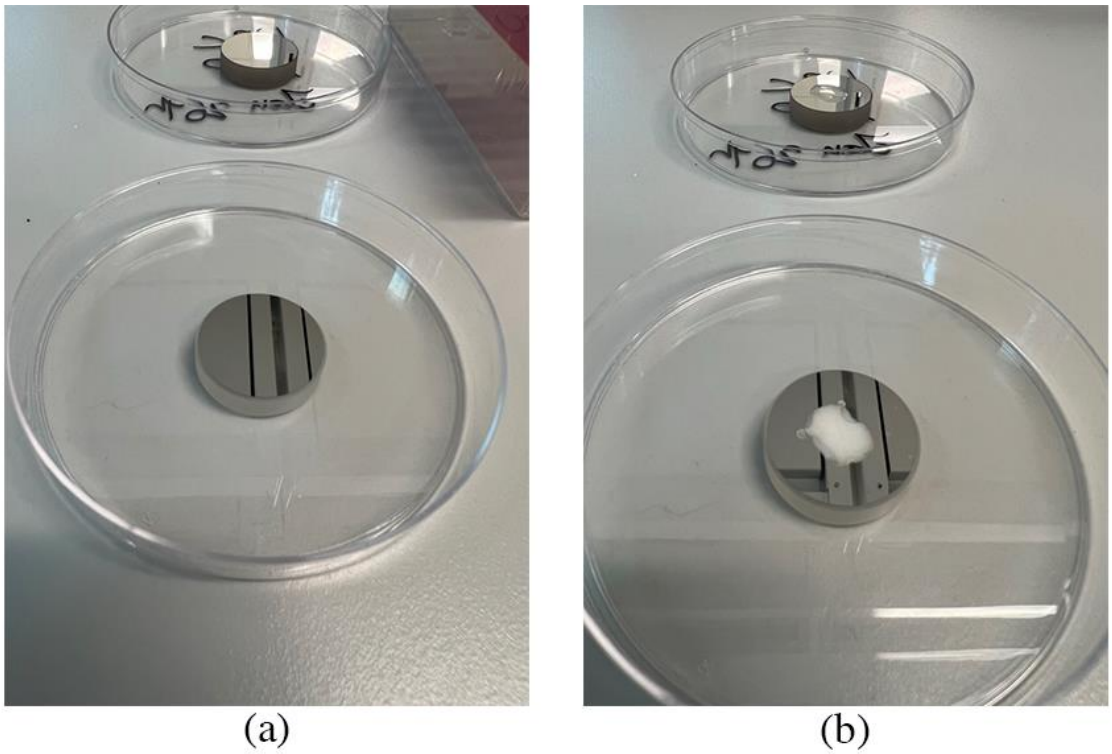

Figure 2-4. (a) The sensing substrate after washing with 70% ethanol (b) Dropcasting MIP mixture on the substrate.

2.5 Gas sensing setup

The gas sensing setup used in this study consists of several components, including a commercial vaporizer (Volcano Hybrid by Storz & Bickel), a specially designed gas sensing chamber, and the sensing substrate itself. The gas sensing set up and exploaded view of its different componets is shown in Figure 2-5.

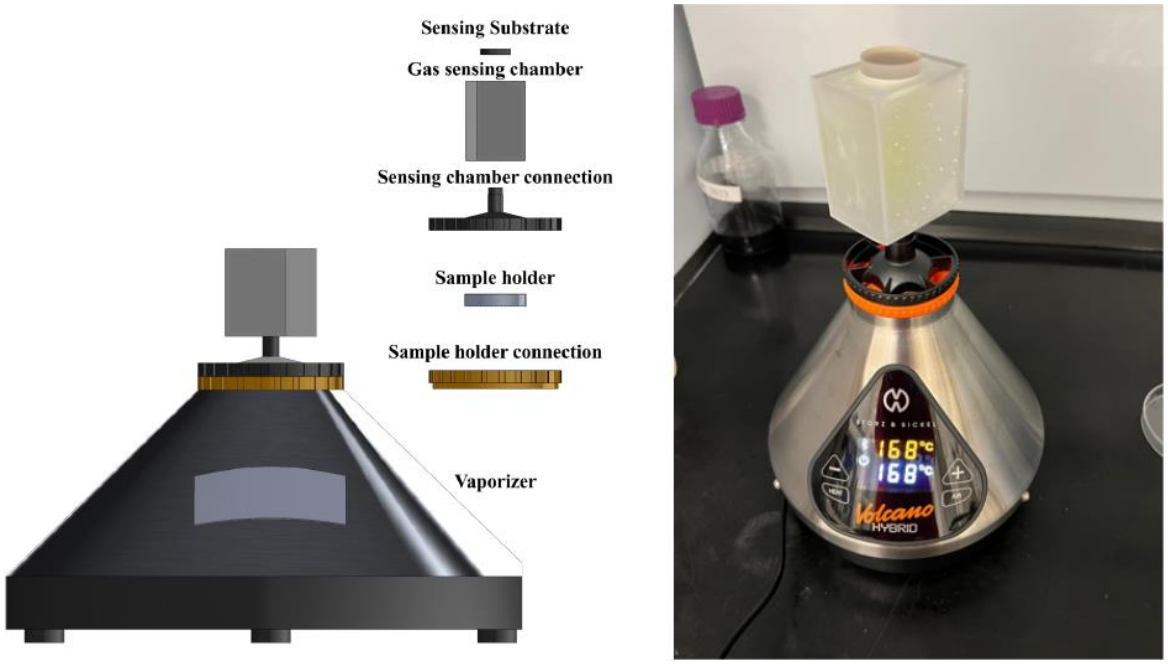

Figure 2-5. Gas sensing set up for exposing analytes.

The gas sensing chamber was designed using SOLIDWORKS 2022 software and was subsequently 3D printed using the Phrozen Sonic Mini Resin 8K 3D printer. The chamber dimensions were precisely designed to accommodate the sensing substrate and facilitate efficient gas sensing experiments. It measures 40.7 mm in width, 55.7 mm in length, and 65.7 mm in height, providing a space for the substrate and ensuring proper gas flow within the chamber.

To create the gas sensing chamber, Anycubic 3D printer clear resin was employed as the printing material. Once the printing process was completed, the chamber was subjected to UV curing for 5 minutes. UV curing enhances the mechanical strength and stability of the printed chamber, ensuring its durability and functionality throughout the gas sensing experiments. By utilizing this 3D-printed gas sensing chamber, it was possible to create a controlled and optimized environment for the gas-sensing measurements, allowing for accurate evaluation of the sensing layer's performance.

After the sensing layer was coated on the substrate as described in section 2.4, the MIP-coated sensing substrate was placed onto the sensing chamber as shown in Figure 2-5, which was then assembled onto the connection. Following this configuration, the MIP-coated substrate was exposed to various concentrations of the analytes of interest.

To achieve specific concentrations of THC and CBD within the sensing chamber, different amounts of these compounds were carefully placed on the sample holder. The sample holder served as a reservoir for the analytes, allowing controlled insertion of specific concentrations into the gas sensing chamber.

To ensure efficient vaporization of THC, the temperature of the vaporizer was set to 180 ℃, which surpasses the vaporization temperature of THC (157 ℃) as indicated in previous research [30]. Similarly, for CBD, the vaporizer temperature was set to 200 ℃, exceeding its vaporization temperature (180 ℃) [30]. By carefully controlling the vaporizer temperature, the analytes were vaporized, allowing their vapors to interact with the MIP-coated sensing substrate within the gas sensing chamber. This experimental setup enabled the investigation and analysis of the response of the MIP-coated substrate to different concentrations of THC, providing insights into detection, sensing, and selectivity capabilities of the sensor.

The sensing mechanism was based on Raman spectroscopy that was subsequently employed to analyze the exposed substrate and gather spectroscopic data.

2.6 Raman spectroscopy based sensing

With the purpose of gas sensing, Raman spectra were acquired over a broad spectral range of 100−3200 cm^{-1} with a high spectral resolution of 3 cm^{-1} using a grating with a density of 2400 lines per millimeter. The Renishaw inVia Raman system, a widely used and reliable instrument,

was employed for the Raman spectroscopy measurements. The excitation laser utilized had a wavelength of 532 nm, providing an appropriate energy level for efficient Raman scattering.

To ensure precise focusing of the laser on the sample, the $20\times$ objective lens connected to the confocal microscope was used for obtaining the results. This configuration allowed for a small laser spot size of 1 μm, enabling localized excitation and enhancing the spatial resolution of the Raman measurements.

The Raman spectra were recorded using the Raman Environment (WiRE) software, which is specifically designed for Raman spectroscopy data acquisition. Subsequently, the obtained spectra were analyzed using Origin Pro 2022b (9.95) software, a powerful and versatile tool for data processing and analysis.

In the process of analyzing the Raman spectra acquired using Origin Pro, the following steps were undertaken:

1. Background Subtraction: The obtained Raman spectra were subjected to background subtraction to eliminate any unwanted signals or noise that could interfere with the accurate interpretation of the data.

2. Smoothing: To enhance the clarity and reduce noise in the spectra, a smoothing technique known as the Savitzky−Golay method was applied. This process effectively improved the overall signal-to-noise ratio and facilitated a clearer representation of the spectral features.

3. Normalization: In order to make a meaningful comparison among the spectra, normalization was performed by referencing all the spectra to the highest peak located at 2948 cm^{-1}. This normalization step allowed for consistent and relative intensity measurements across different samples.

By implementing these procedures, the Raman spectra were effectively pre-processed and prepared for further analysis, ensuring reliable and accurate insights into the molecular and structural characteristics of the samples under investigation.

To account for variations in the measurements, the MIP sensor was exposed to each concentration of interest once. However, to ensure robustness and statistical confidence in the obtained results, Raman spectra were collected from five different spots on the sensor after each exposure. This approach allowed for a comprehensive analysis of the sensor's response at each concentration, while also capturing any spatial variations in the spectral features. Consequently, the data obtained from multiple spots on the sensor provided a representative and consistent assessment of the analytes being detected. This procedure was similarly repeated for NIP sensor as well.

Also, to maintain consistency throughout the measurements, the experimental parameters such as laser power and exposure time were kept constant at 100% and 10 s, respectively. This practice ensured that any observed differences in the obtained spectra were predominantly attributed to variations in the analytes being studied rather than fluctuations in the experimental conditions.

Chapter 3: Results and Discussion

In this section, the experimental results obtained from the analysis of MIPs combined with Raman spectroscopy for the selective detection of THC is presented. The results are organized into two sections: the first part focuses on the SEM analysis and Raman characterization, which reveals the morphological features, surface characteristics, size distribution, and molecular fingerprint of the MIPs and NIPs, while the second part highlights the Raman sensing data, demonstrating the usefulness of MIP-based sensors in the specific detection of THC. The combination of these two techniques provides comprehensive insights into the design and performance of MIPs for THC detection, thereby establishing a solid foundation for their potential applications in quality control in the cannabis industry, and other relevant fields.

3.1 Characterization results

3.1.1 SEM

SEM analysis was employed to investigate the morphological properties and surface characteristics of the MIP and NIP nanoparticles synthesized in this study. The SEM images obtained provide crucial insights into the structural features and surface topography of the nanoparticles, which are pivotal in determining their recognition capabilities and overall performance as selective sensors for THC.

3.1.1.1 MIPs

Figure 3-1 (a-c) illustrates the SEM images of the MIP nanoparticles, revealing a well-defined morphology with distinct features. The MIP nanoparticles are spherically shaped with a uniform size distribution, with an average size of 163±23 nanometers in diameter shown in Figure 3-1 (d). The SEM analysis also confirms the presence of surface irregularities across the nanoparticle surface. These features contribute to an increased surface area, facilitating stronger interactions

between the MIP nanoparticles and THC molecules, thereby enhancing their recognition capabilities.

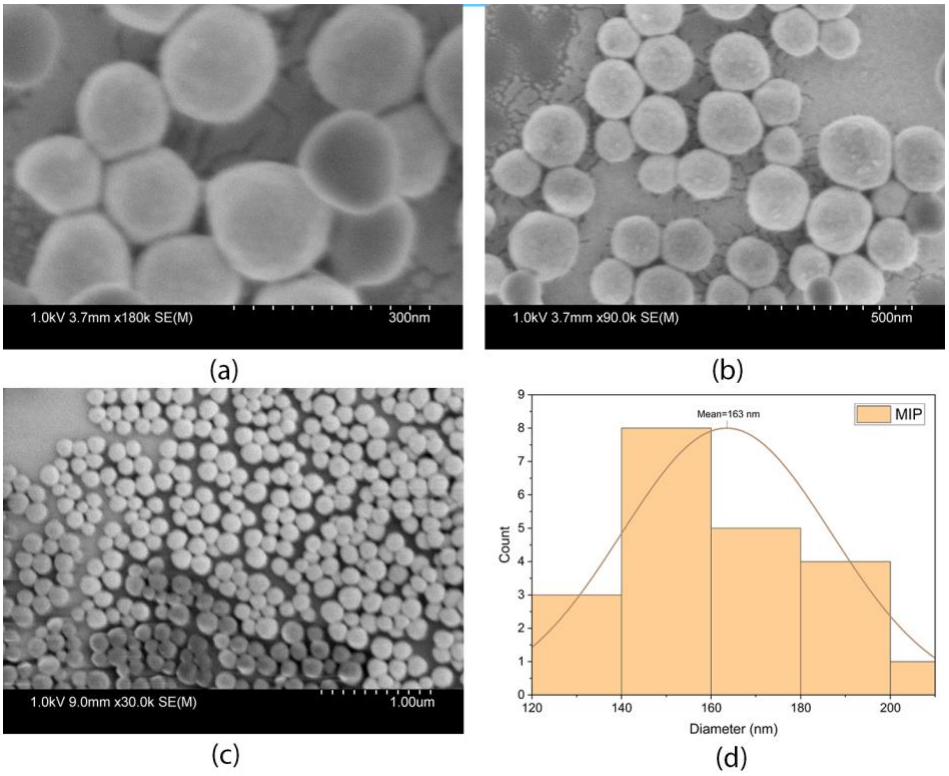

Figure 3-1. (a-c) SEM images of MIP NPs (d) Size distribution of the fabricated MIP NPs.

3.1.1.2 NIPs

In contrast, Figure 3-2 (a-c) showcases the SEM image of the NIP nanoparticles, which were synthesized under identical conditions to the MIP nanoparticles but in the absence of the template molecule. The NIP nanoparticles exhibit a smooth and featureless surface, lacking the irreguralities observed in the MIP nanoparticles. The NIP nanoparticles have a uniform size distribution, with an average size of 642±48 nanometers in diameter shown in Figure 3-2 (d). This observation further confirms the successful imprinting of THC molecules within the MIP nanoparticles, as evident from the morphological differences between the MIP and NIP nanoparticles.

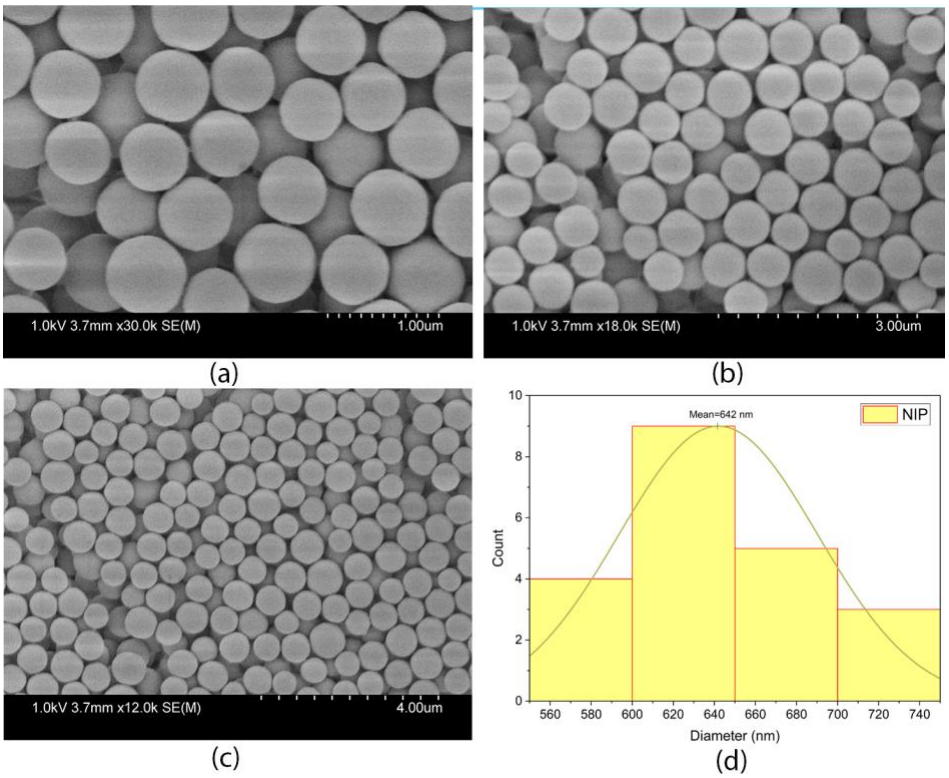

Figure 3-2. (a-c) SEM images of NIP NPs (d) Size distribution of the fabricated NIP NPs.

Overall, the SEM results demonstrate the successful synthesis of MIP nanoparticles with well-defined morphologies and distinct surface features, highlighting their potential as selective platforms for THC detection. The distinct morphological differences observed between the MIP and NIP nanoparticles emphasize the importance of molecular imprinting in creating specific recognition sites for THC within the nanoparticle matrix.

A noticeable difference inside MIP and NIP NPs SEM pictures is size difference. During MIP synthesis, the template molecule plays a crucial role in guiding polymerization, acting as a molecular mold that shapes specific binding sites within the polymer. These sites are designed to complement the template's shape and functionality, resulting in smaller and more defined structures compared to NIPs. The presence of the template creates specific cavities within the polymer matrix, responsible for selective recognition and binding of the target molecule or similar molecules. This reduction in particle volume leads to smaller sizes compared to NIPs.

Additionally, the cross-linking density of the polymer network can be influenced by the presence of the template, affecting the overall structure. After synthesis, the template is removed from the MIPs, leaving behind the selective cavities or binding sites. This process further contributes to the size reduction and formation of specific recognition sites in the MIP particles. In various studies investigating MIPs and NIPs, a significant disparity in size was observed between the two types of polymers. This variation can be attributed to multiple factors, including template-induced polymerization, the cross-linking process employed during MIP synthesis (which affects polymer density), and the presence and subsequent removal of the template molecule. These factors collectively contribute to the distinct size differences observed between MIPs and NIPs across the reported studies [84]–[87].

These findings provide a solid foundation for further investigations into the performance and optimization of MIP-based sensors for THC detection.

3.1.2 Raman spectroscopy

Raman spectroscopy was employed to characterize the NIPs and MIPs, both before and after template removal. The Raman spectra obtained provide valuable insights into the vibrational properties and chemical composition of the polymers, allowing for a comprehensive analysis of their selective detection capabilities for THC.

Figure 3-3 presents the Raman spectrum of the NIPs and MIPs before and after template removal. The spectrum of MIP before template removal shows several characteristic peaks associated with the polymer matrix. Notably, a major peak is observed at 1614 cm^{-1}, which is absent in the corresponding spectrum of the MIPs after template removal. This distinctive peak indicates the presence of the template THC molecules that was used during the imprinting process, resulting in the formation of specific binding sites within the MIPs.

In comparison, the Raman spectrum of the NIPs displays similar vibrational peaks to those observed in the MIPs before template removal. However, the absence of the prominent peak at 1614 cm^{-1} suggests that the NIPs lack the specific binding sites for THC, further confirming the significance of molecular imprinting in creating selective recognition sites within the MIPs.

Interestingly, upon template removal, the Raman spectrum of the MIPs exhibits a profile that closely resembles that of the NIPs. The disappearance of the peak at 1614 cm^{-1} in the MIP spectrum after template removal indicates the successful removal of the template THC molecules from the polymer matrix. This observation validates the efficiency of the washing process in eliminating the template molecules while preserving the structural integrity of the MIPs.

The similarity between the Raman spectra of the NIPs and the washed MIPs suggests that the MIPs have successfully retained their overall structural and vibrational characteristics, with the removal of the template THC molecules being the primary distinction between the two. This finding indicates that the MIPs have retained their inherent recognition capabilities even after template removal, further emphasizing their potential for selective THC detection.

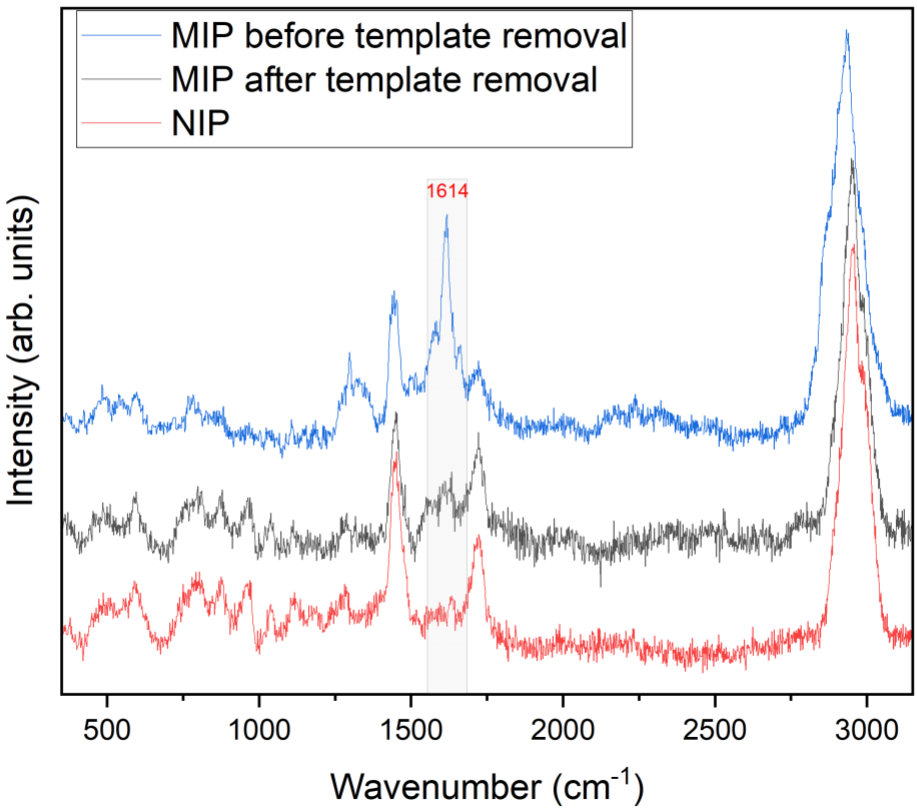

Figure 3-3. Raman spectrum of MIP NPs before and after wash and NIP NPs.

The wavenumber of the major peaks observed in the Raman spectra and their corresponding bonds are listed in Table 3-1 [88].

Table 3-1. Major peaks in Raman spectra of MIP (after and before template removal) and NIP NPs and their corresponding bonds

Peak Wavenumber (cm^{-1})	Material	Corresponding bond
2937	MIP before template removal	C-H
1724	MIP before template removal	C=O
1614	MIP before template removal	C=C
1445	MIP before template removal	C-H or C-C

2948	MIP after template removal	C-H
1724	MIP after template removal	C=O
1449	MIP after template removal	C-H or C-C
2959	NIP	C-H
1725	NIP	C=O
1449	NIP	C-H or C-C

Overall, the Raman characterization results confirm the successful imprinting of THC molecules within the MIPs, as evidenced by the distinctive peak at 1614 cm^{-1} in the MIP spectrum before template removal. The disappearance of this peak in the washed MIP spectrum indicates the effective removal of the template, while the resemblance between the Raman spectra of the washed MIPs and the NIPs highlights the selective recognition properties of the MIPs. These findings provide essential insights into the design and performance of MIP-based sensors for THC detection and pave the way for further optimization and applications in the field of cannabis analysis.

3.2 Gas sensing results

In this section, the results obtained from the gas sensing experiments using MIPs and NIPs for the detection of THC is presented. The gas sensing results are divided into three parts: the Raman spectra of the MIPs exposed to different concentrations of THC, the Raman spectra of the NIPs exposed to the same various concentrations of THC, and the calibration plot illustrating the relationship between THC concentration and the corresponding Raman intensity.

3.2.1 Raman spectra of MIP exposed to THC

The Raman spectra of the MIPs exposed to various concentrations of THC provide valuable insights into the response of the MIP-based sensor towards the target analyte. The substrates were

exposed to THC vapor ranging from 250 to 3500 ppm, and the resulting characteristic signals caused by THC binding to the MIP-coated surface were measured.

Figure 3-4 displays the Raman spectra obtained from the MIPs upon exposure to increasing concentrations of THC. The spectra exhibit a distinct change in the vibrational peaks as a function of THC concentration, indicating the sensitivity of the MIPs towards THC. This distinct change is the addition of a peak at the wavenumber of 1614 cm^{-1}.

As it was seen before in section 2.6, the Raman spectrum of the MIP-coated substrate exhibited significantly enhanced peaks at specific wavenumbers, namely 2948 cm^{-1}, 1724 cm^{-1}, and 1449 cm^{-1}. These enhanced peaks are indicative of the presence of functional groups and structural elements within the MIP that are involved in the binding and interaction with THC.

Upon exposure to THC, a new peak appeared at 1614 cm^{-1} (highlighted with a vertical yellow box) in the Raman spectrum of the MIP-coated substrate. This new peak corresponds to the vibrations of the benzene ring in the chemical structure of THC. The appearance of this peak further confirms the selective binding of THC molecules to the MIP surface. Moreover, as the concentration of THC increased, the intensity of the peaks corresponding to the enhanced Raman signals also increased proportionally. This correlation between THC concentration and peak intensity demonstrates the sensitivity of the MIP-based sensor in detecting and quantifying THC.

At higher concentrations of THC, additional vibrational bands originating from THC were observed in the Raman spectrum of the MIP-coated substrate. These bands appeared at 1304 cm^{-1} and corresponded to the ring stretch and twist of the benzene ring, C-OH bend, CH & CH2 bend, and C-O stretch (tetrahydropyran ring) [89]. These vibrational bands provide further evidence of the selective interaction between THC and the MIP surface, indicating the specific recognition and binding of THC by the imprinted sites within the MIP.

In addition, to assess the reusability of the MIP-coated substrate, the sensing surface was tested five times after exposure to each concentration of the analyte. Remarkably, even after five repetitions, the MIP-coated surface still exhibited the same response to THC, suggesting that the MIP nanoparticles retained their specific binding capabilities. This finding indicates the durability and robustness of the MIP-based sensor for repeated THC detection. As an example Table 3-2 includes the wavenumber of the major peaks for the raman spectra taken from five different spots of the MIP-coated substrate exposed to 1000 ppm of THC.

Table 3-2. Wavenumber analysis of major peaks in the five Raman Spectra taken from MIP exposed to 1000 ppm of THC

Peaks	Spectrum 1	Spectrum 2	Spectrum 3	Spectrum 4	Spectrum 5	Mean	SD	RSD
Peak #1 (cm^{-1})	1450	1454	1449	1449	1449	1450.2	2.167948	0.149493
Peak #2 (cm^{-1})	1613	1615	1610	1615	1616	1613.8	2.387467	0.147941
Peak #3 (cm^{-1})	1725	1725	1725	1725	1729	1725.8	1.788854	0.103654
Peak #4 (cm^{-1})	2952	2950	2950	2950	2954	2951.2	1.788854	0.060614

From the Raman spectral analysis results of the peaks in five spectra obtained from MIP exposed to 1000 ppm of THC, it can be concluded that the spectra demonstrate a high degree of similarity. The small standard deviations (SD) and low relative standard deviation (RSD), further support the conclusion that the peaks in these spectra are highly consistent and reliable. These findings suggest

that the MIP-based Raman sensor is capable of providing consistent and accurate results, demonstrating its potential for selective detection of THC.

In summary, the gas sensing experiments utilizing the MIP-coated substrate demonstrated the successful detection of THC at different concentrations. The enhanced Raman peaks and the appearance of a new peak at 1614 cm^{-1} confirmed the specific binding of THC to the MIP surface. The intensity of the peaks increased with increasing THC concentration, providing a basis for quantification. The additional vibrational bands observed at higher concentrations further supported the selective recognition of THC by the MIP surface. These results highlight the potential of MIP-based gas sensing platforms for the selective and sensitive detection of THC in various applications.

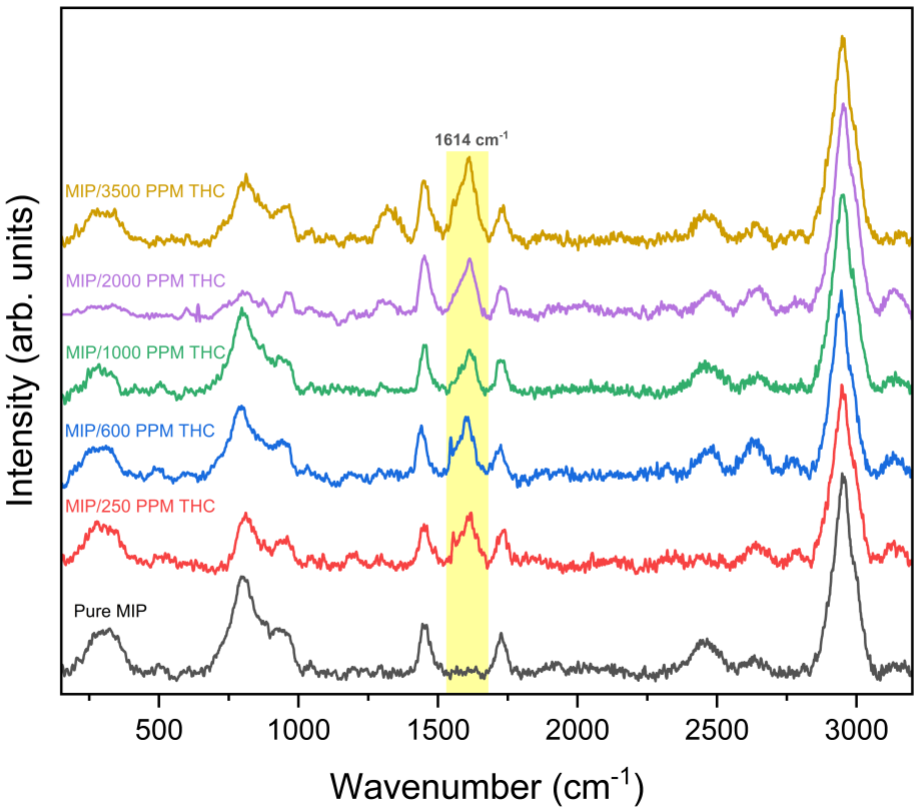

Figure 3-4. Normalized Raman spectra of the MIP-coated surface before and after binding THC at different concentrations (five different spots analyzed on the sensing layer for each concentration).

3.2.2 Raman spectra of NIP exposed to THC

To assess the specificity of the MIP-based sensor, the Raman spectra of the NIPs exposed to THC were also recorded. Figure 3-5 presents the Raman spectra obtained from the NIPs upon exposure to THC at the same concentration range of MIPs' (250 to 3500 ppm). A closer examination of the spectrum reveals strongly enhanced peaks at 2959 cm^{-1}, 1725 cm^{-1}, and 1449 cm^{-1}, which are characteristic of the NIP normal Raman spectrum.These enhancements can be attributed to the intrinsic vibrational properties of the NIP material [88].

Interestingly, the spectrum also shows an enhancement of a peak at 1614 cm^{-1} (highlighted with a vertical yellow box) in the NIPs exposed to THC. This peak exhibits similar characteristics to the

THC-induced peak observed in Figure 3-4, which corresponds to the vibrations of the benzene ring in THC's chemical structure. However, it is important to note that the relative intensity of the peaks at 1614 cm^{-1} in the NIPs is lower compared to the corresponding peaks in the MIPs exposed to THC.

In this context, the MIP nanoparticles served as affinity adsorbents with specific binding sites designed to capture THC and bring the analyte in close proximity to the underlying Raman active substrate. Consequently, the MIP-coated surface generated a strong and characteristic signal in response to THC. On the other hand, the NIP-coated surface exhibited a much weaker signal due to the absence of high-affinity binding sites for THC. This result highlights the selective nature of the MIP-based sensor, which possesses specific recognition sites for THC, resulting in a more noticeable response compared to the NIP-based sensor.

Same as with MIP-coated surface, the NIP-coated sensing surface was tested five times after exposure to each concentration of the analyte. As an example Table 3-3 includes the wavenumber of the major peaks for the raman spectra taken from five different spots of the MIP-coated substrate exposed to 1000 ppm of THC.

Table 3-3. Wavenumber analysis of major peaks in the five Raman Spectra taken from NIP exposed to 1000 ppm of THC

Peaks	Spectrum 1	Spectrum 2	Spectrum 3	Spectrum 4	Spectrum 5	Mean	SD	RSD
Peak #1 (cm^{-1})	1440	1445	1446	1444	1443	1443.6	2.302173	0.159474
Peak #2 (cm^{-1})	1613	1611	1615	1612	1614	1613	1.581139	0.098025

Peak #3 (cm^{-1})	1721	1722	1723	1720	1724	1722	1.581139	0.09182
Peak #4 (cm^{-1})	2956	2958	2955	2957	2954	2956	1.581139	0.053489

Based on the analysis of Raman spectral peaks from five spectra of NIP exposed to 1000 ppm of THC, it can be inferred that these spectra exhibit a strong resemblance. The presence of small standard deviations (SD) and low relative standard deviation (RSD) provides additional evidence for the consistent and reliable nature of these peaks.

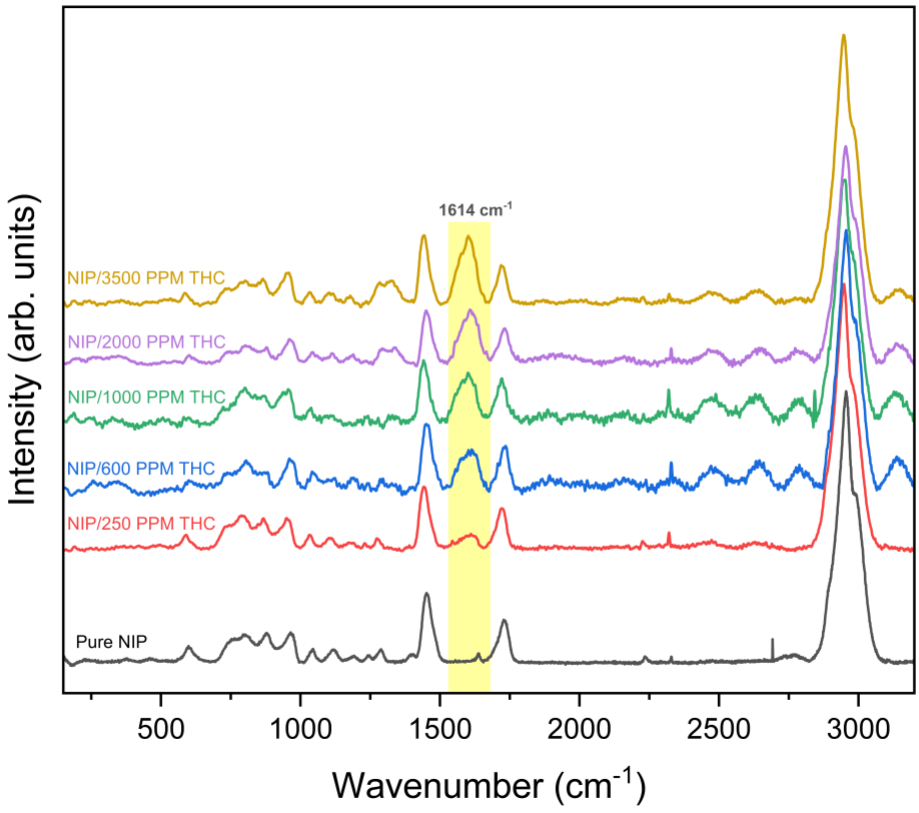

Figure 3-5. Normalized Raman spectra of the NIP-coated surface before and after binding THC at different concentrations (five different spots analyzed on the sensing layer for each concentration).

3.2.3 Calibration plot

To analyze the quantitative relationship between THC concentration and the corresponding Raman intensity, a calibration plot was constructed. This was achieved by normalizing the THC signal at 1614 cm^{-1}, which corresponds to the vibrations of the benzene ring in THC's chemical structure, against the highest intense band of the MIP at 2948 cm^{-1}. The same normalization procedure was applied to both the MIP- and NIP-coated surfaces.

Figure 3-6 illustrates the calibration plot that was obtained from the Raman spectra of exposed MIP and NIP substrates. The results indicate that the MIP-coated surface produced a significantly higher analytical signal compared to the NIP-coated surface. This finding highlights the superior performance and sensitivity of the MIP-based sensor for THC detection. In summary, the results from this section demonstrate that the NIP-based sensor generates a weaker response to THC, as evidenced by the lower intensity of the THC-induced peak at 1614 cm^{-1}. In contrast, the MIP-based sensor exhibits a stronger and specific response to THC due to the presence of high-affinity binding sites.

The calibration plot exhibits a correlation between the THC signal and concentration within the range of 250 to 3500 ppm. Although the raw data may not appear strictly linear, it can be effectively linearized through suitable data transformation or mathematical treatment. The high coefficient of determination (R-square) value of 0.94 further supports the strong relationship between THC concentration and the resulting Raman intensity after linearization. As the concentration of THC increases, the Raman signal also increases proportionally, allowing for the quantitative determination of THC concentration. Also, the calibration curve is used to understand the response to THC at different concentrations, and predict the concentration in an unknown

sample. The data are fitted with a linear function, so that unknown concentrations of THC in the reported range can be predicted. Our calibration curve shows the limit of detection at the order of 250 ppm.

It is worth noting that at the highest concentration of THC (3500 ppm), there may be instances where THC molecules adsorb onto the surface through nonspecific binding. This nonspecific adsorption can contribute to an increased Raman signal, further emphasizing the sensitivity of the MIP-based sensor.

In summary, the calibration plot obtained from the gas sensing experiments demonstrates the dose-response relationship between THC concentration and the corresponding Raman intensity. The MIP-coated surface consistently outperforms the NIP-coated surface in generating a higher analytical signal, indicating the sensitivity and affinity of the MIP-based sensor towards THC. The almost linear increase in the THC signal within the tested concentration range provides a basis for quantifying THC concentrations using the Raman intensity. These findings validate the potential of the MIP-based gas sensing platform as a reliable tool for the accurate detection and measurement of THC in various applications such as quality control in the cannabis industry, and other relevant fields.

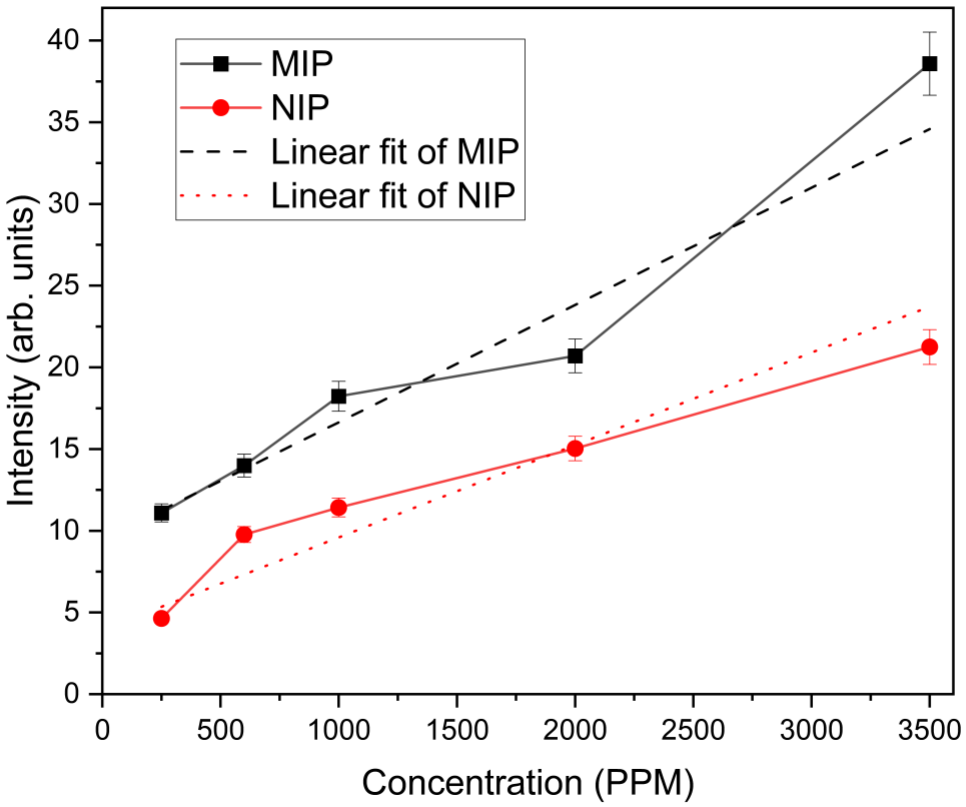

Figure 3-6. The calibration curve constructed by plotting the intensity of the THC peak at 1614 cm^{-1} against concentration, measured using both MIP- and NIP-coated substrates.

3.3 Selectivity analysis

To assess the selectivity of the MIP-based sensor, it was exposed to various compounds including cannabidiol (CBD), acetone, and ethanol. The objective of this experiment was to investigate the response of the MIP sensor to these different analytes and assess its ability to selectively detect Δ^9-tetrahydrocannabinol (THC).

CBD, a compound structurally similar to THC, was included in the study to examine the sensor's capability to distinguish between these two molecules accurately. This is particularly important in applications where differentiation between THC and CBD is essential for quality control and identification purposes. Additionally, the response of the sensor to acetone and ethanol was

analyzed to determine whether these common solvents, which may be used to dissolve THC and CBD, would interfere with the sensor's detection performance.

In the subsequent section, the results obtained from the gas sensing experiments involving CBD, acetone, and ethanol, providing valuable insights into the selectivity and performance of the MIP-based sensor are presented and discussed.

3.3.1 Selectivity to CBD

To demonstrate the MIP-based Raman sensor's ability to detect THC in the presence of potential interfering compounds, a series of experiments were conducted. To start, the MIP-coated surface was exposed to cannabidiol (CBD) with the concentration of 1000 ppm and raman spectrum was recorded.

The Raman spectra analysis, as depicted in Figure 3-7, revealed that CBD, being an organic amine, could undergo physisorption onto the MIP-coated surface containing carboxyl groups. This interaction generated a distinct Raman band at 1622 cm^{-1}, corresponding to C-C (in-plane) stretch, C-H bend, and O-H bend [89]. Despite this interference from CBD, the THC signal at 1614 cm^{-1} is still readily detectable. This result demonstrates the capability of Raman spectroscopy as a fingerprint identification technique to overcome the cross-reactivity issue often associated with molecularly imprinted polymers. Combining the selectivity of MIPs with the molecular identification power of Raman spectroscopy produces a synergistic effect, leading to more reliable and accurate analytical results.

Figure 3-7 further provides a visual representation of the chemical structures of THC and its analog CBD. Among the compounds investigated, THC and CBD exhibit the most similar chemical structures, differing only in the number of hydrogen atoms present in their respective benzene rings.

By successfully and selectively detecting THC from CBD, the MIP-based Raman sensor demonstrates its effectiveness in providing selective and accurate identification of target analytes. This finding reinforces the potential of combining molecularly imprinted polymers and Raman spectroscopy as a robust and reliable analytical approach in various fields, including forensic analysis, quality control, and other applications where precise discrimination of closely related compounds like THC and CBD is essential.

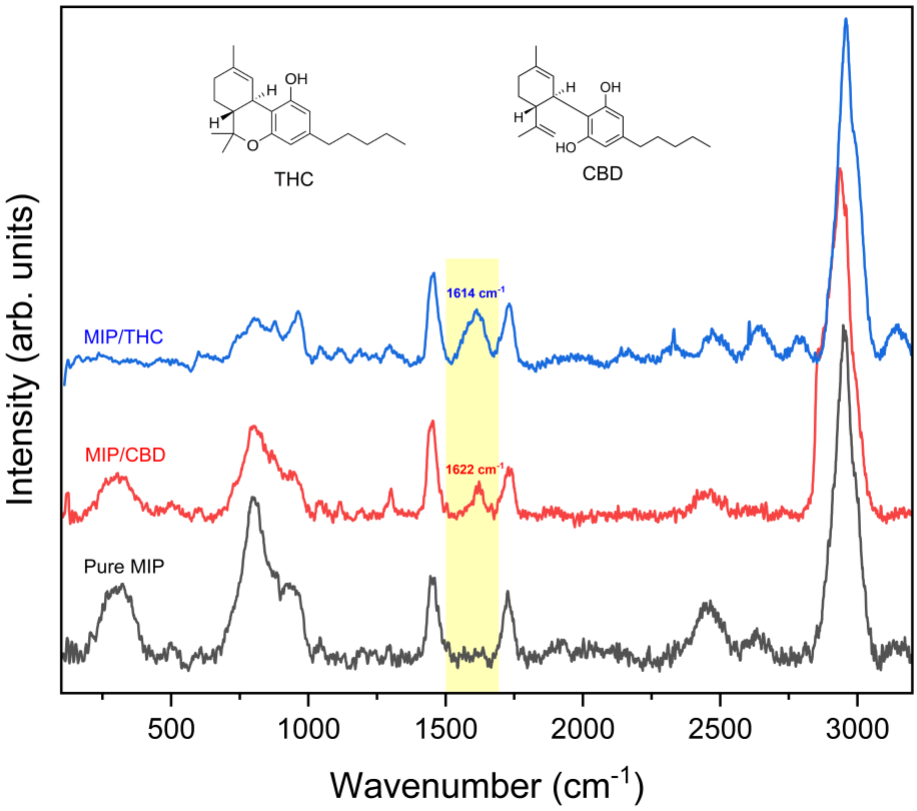

Figure 3-7. Comparison of Raman spectra recorded from MIP-coated surface exposed to CBD and THC including the chemical structure of THC and CBD (Both 1000 ppm).

3.3.2 Selectivity to acetone and ethanol

The selectivity of the MIP-based Raman sensor to ethanol, acetone, and THC was investigated by analyzing the Raman spectra recorded on an MIP-coated surface exposed to these substances, all at a concentration of 500 ppm. Figure 3-8 illustrates the obtained spectra.

Upon examination of the spectra, no additional peaks beyond the characteristic MIP spectrum associated with ethanol and acetone at 500 ppm were observed. This indicates that using Raman spectroscopy, it was not possible to detect ethanol and acetone at this concentration range. Alternatively, it suggests that the MIP's selective binding sites may not be suitable for the adsorption of volatile organic compounds (VOCs) such as ethanol and acetone.

The absence of distinct peaks related to ethanol and acetone in the recorded Raman spectra supports the notion that the MIP-based sensor exhibits selectivity towards THC while showing limited affinity towards these interfering compounds. This finding further demonstrates the sensor's specificity for detecting THC, highlighting its potential for accurate and reliable identification in scenarios where THC detection is of particular importance.

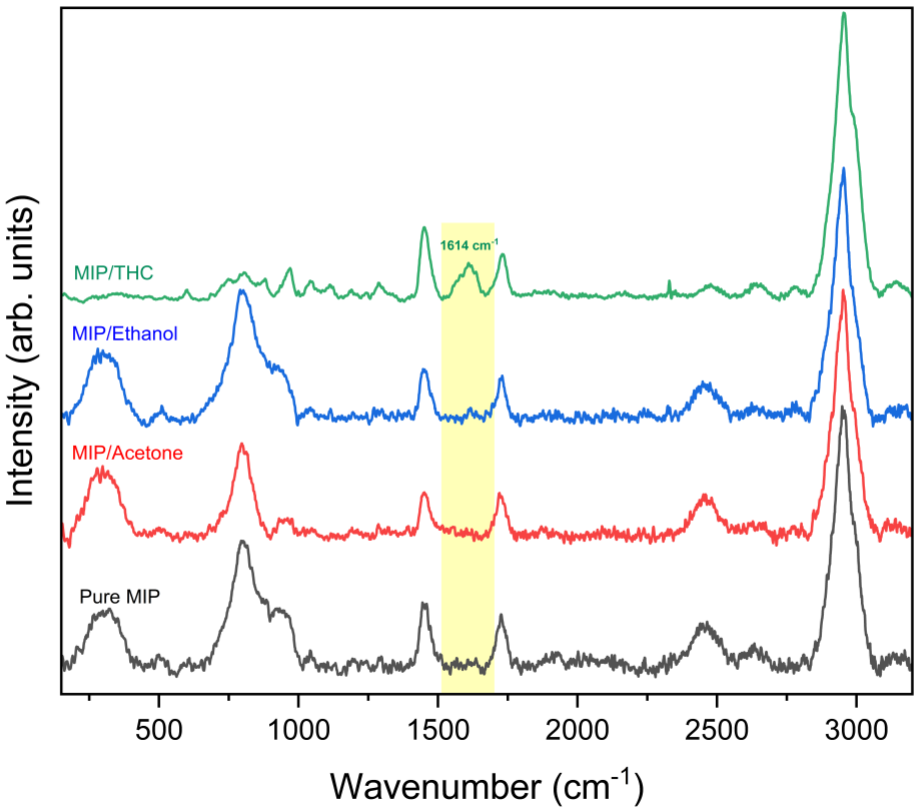

Figure 3-8. Comparison of Raman spectra recorded from MIP-coated surface exposed to ethanol, acetone, and THC (All at 500 ppm).

Chapter 4: Conclusion

4.1 Summary

This study presents the development of a novel sensor for the sensitive and selective detection of Trans-Δ^9-tetrahydrocannabinol (THC) using a molecularly imprinted polymer (MIP) synthesized with a THC template. The sensor combines MIP technology with Raman spectroscopy to achieve label-free monitoring of THC. The MIP sensor exhibits a prominent peak at 1614 cm^{-1} in the Raman spectrum, attributed to the THC target molecule, enabling the selective quantification of bound THC with a low detection limit of 250 ppm. The sensor's functionality is further demonstrated through comparative studies with a non-imprinted polymer (NIP) control and analysis of the Raman spectrum of MIP exposed to Cannabidiol (CBD), ethanol, and acetone. The study also delves into the synthesis process of MIPs, providing a detailed explanation of the steps involved, from mixing and polymerization to sonication for template removal and MIP and NIP NPs separation. The graphical abstract of this study is shown in Figure 4-1.

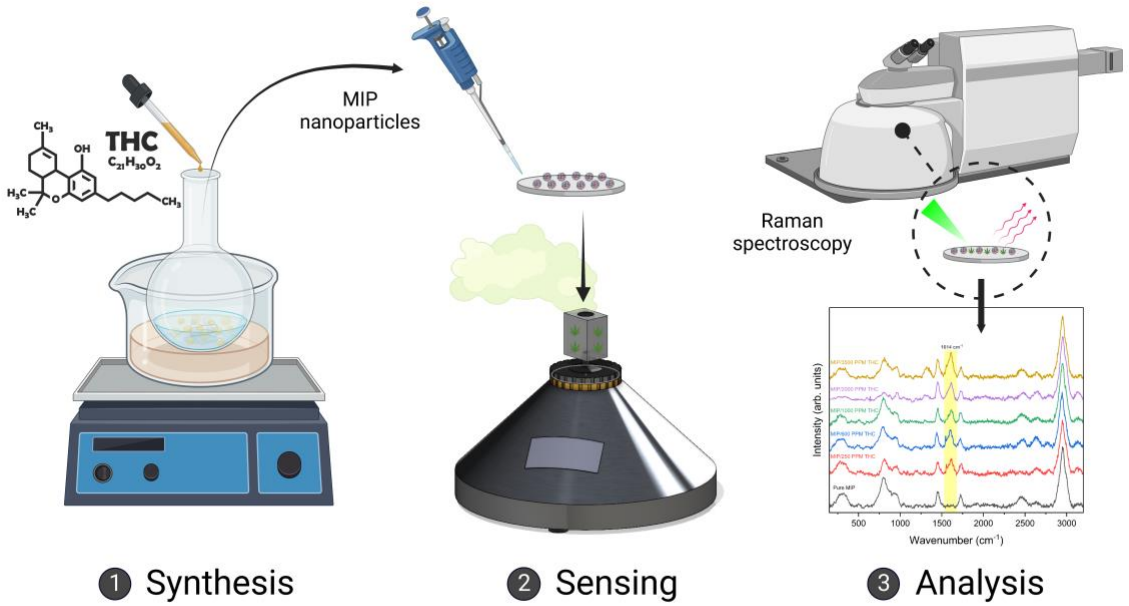

Figure 4-1. Summary of the study shown in three sections: synthesis, gas sensing, and analysis.

In Table 4-1, we present previous work on detection of various target analyses using combination of Raman-based sensing and MIPs. While the previous research has primarily focused on various target analytes using Surface-enhanced Raman Scattering (SERS) techniques, this thesis introduces an approach by employing standard Raman-based sensing combined with MIPs for THC gas sensing for the first time. Notably, this work achieves a detection limit of 250 ppm for THC gas, demonstrating the potential of Raman-based MIPs in gas sensing applications.

Table 4-1. Comparison of detection limits for different target analytes using Raman-based sensing and MIPs

Target Analyte	Technique	Detection Limit	References
(S)-propranolol	SERS and MIP	$10^{-7}M$	[76]
Bisphenol A	SERS and MIP	$10^{-9}M$	[74]
2, 6-dichlorophenol	SERS and MIP	$10^{-9}\ mol\ L^{-1}$	[90]
THC	Normal Raman and MIP (This Work)	250 ppm	This Thesis

4.2 Contributions

The study has made several significant contributions:

- Synthesized MIP and NIP nanoparticles and presented the characterization methods, sensor preparation, and gas sensing setup.
- Conducted characterization tests to understand the morphology, size distribution, and chemical composition, and other properties of the synthesized materials.

- Demonstrated the successful synthesis of MIP nanoparticles with well-defined morphologies and distinct surface features, highlighting their potential as selective platforms for THC detection.
- Developed a gas sensing setup to evaluate the performance of the MIP/NIP sensor for THC detection
- Employed Raman spectroscopy to characterize the NIPs and MIPs, both before and after template removal, synthesized in this study.
- Combined MIP technology with Raman spectroscopy to achieve label-free monitoring of THC based on a single identifying Raman peak
- Constructed a calibration plot to analyze the quantitative relationship between THC concentration and the corresponding Raman intensity.
- Analyzed the selectivity of the MIP-based sensor to CBD which has a similar molecular structure to THC.

4.3 Future Work

While this thesis has focused on the development of a proof-of-concept sensor for the sensitive and selective detection of Trans-Δ^9-tetrahydrocannabinol (THC) using MIP combined with Raman spectroscopy, there are several avenues for future research and development in this field. The possible future works include:

- Portable and Miniaturized Device: One potential direction for future work is the miniaturization and portability of the sensor. Currently, the sensor operates in a laboratory setting with benchtop Raman spectroscopy equipment. To enhance its practicality and applicability, efforts should be made to integrate the MIP sensor with handheld portable

Raman devices. This would enable on-site and real-time THC detection in various scenarios, such as forensic investigations or field testing.

- Detection of Lower Concentrations: Another area for future exploration is improving the detection sensitivity of the sensor, particularly for lower concentrations of THC. Surface-enhanced Raman scattering (SERS) techniques have shown great potential in enhancing the Raman signal and improving detection limits. Incorporating SERS techniques into the MIP sensor could enable the detection of THC at even lower concentrations, expanding its range of applications and increasing its analytical capabilities.
- Detection in Plasma, Saliva, and Other Biological Media: While this thesis has focused on gas-phase detection of THC, future studies could investigate the detection of THC in plasma, saliva, and other biological media. These matrices pose additional challenges due to their complex compositions and potential interference from other compounds. Adapting the MIP sensor and optimizing the sample preparation and analysis techniques for these media would broaden the scope of THC detection, enabling applications in clinical diagnostics, drug testing, and pharmacokinetic studies.

In conclusion, future work in this field should focus on miniaturizing the MIP sensor for portable use, improving detection sensitivity using SERS techniques, and expanding the application of the sensor to detect THC in various biological media. These advancements will contribute to the development of more practical, sensitive, and versatile THC detection methods, opening up new possibilities for forensic, medical, and pharmaceutical applications.

Bibliography

[1] J. W. Lowdon *et al.*, "Engineering molecularly imprinted polymers (MIPs) for the selective extraction and quantification of the novel psychoactive substance (NPS) methoxphenidine and its regioisomers," *Analyst*, vol. 143, no. 9, pp. 2002–2007, 2018, doi: 10.1039/C8AN00131F.

[2] J. W. Lowdon *et al.*, "MIPs for commercial application in low-cost sensors and assays - An overview of the current status quo," *Sens. Actuators B Chem.*, vol. 325, p. 128973, Dec. 2020, doi: 10.1016/j.snb.2020.128973.

[3] D. Refaat *et al.*, "Strategies for Molecular Imprinting and the Evolution of MIP Nanoparticles as Plastic Antibodies—Synthesis and Applications," *Int. J. Mol. Sci.*, vol. 20, no. 24, p. 6304, Dec. 2019, doi: 10.3390/ijms20246304.

[4] J. J. BelBruno, "Molecularly Imprinted Polymers," *Chem. Rev.*, vol. 119, no. 1, pp. 94–119, Jan. 2019, doi: 10.1021/acs.chemrev.8b00171.

[5] V. B. Kandimalla and H. Ju, "Molecular imprinting: a dynamic technique for diverse applications in analytical chemistry," *Anal. Bioanal. Chem.*, vol. 380, no. 4, pp. 587–605, Oct. 2004, doi: 10.1007/s00216-004-2793-9.

[6] Y. Zhang, J. Zhang, and Q. Liu, "Gas Sensors Based on Molecular Imprinting Technology," *Sensors*, vol. 17, no. 7, Art. no. 7, Jul. 2017, doi: 10.3390/s17071567.

[7] M. Irshad *et al.*, "Molecularly Imprinted Nanomaterials for Sensor Applications," *Nanomaterials*, vol. 3, no. 4, pp. 615–637, Nov. 2013, doi: 10.3390/nano3040615.

[8] L. Figueiredo, G. L. Erny, L. Santos, and A. Alves, "Applications of molecularly imprinted polymers to the analysis and removal of personal care products: A review," *Talanta*, vol. 146, pp. 754–765, Jan. 2016, doi: 10.1016/j.talanta.2015.06.027.

[9] M. Marć and P. P. Wieczorek, "Chapter One - Introduction to MIP synthesis, characteristics and analytical application," in *Comprehensive Analytical Chemistry*, M. Marć, Ed., in Mip Synthesis, Characteristics and Analytical Application, vol. 86. Elsevier, 2019, pp. 1–15. doi: 10.1016/bs.coac.2019.05.010.

[10] W. J. Cheong, S. H. Yang, and F. Ali, "Molecular imprinted polymers for separation science: A review of reviews," *J. Sep. Sci.*, vol. 36, no. 3, pp. 609–628, 2013, doi: 10.1002/jssc.201200784.

[11] P. A. G. Cormack and A. Z. Elorza, "Molecularly imprinted polymers: synthesis and characterisation," *J. Chromatogr. B*, vol. 804, no. 1, pp. 173–182, May 2004, doi: 10.1016/j.jchromb.2004.02.013.

[12] J. Wackerlig and P. A. Lieberzeit, "Molecularly imprinted polymer nanoparticles in chemical sensing – Synthesis, characterisation and application," *Sens. Actuators B Chem.*, vol. 207, pp. 144–157, Feb. 2015, doi: 10.1016/j.snb.2014.09.094.

[13] G. Vasapollo *et al.*, "Molecularly imprinted polymers: present and future prospective," *Int. J. Mol. Sci.*, vol. 12, no. 9, pp. 5908–5945, 2011, doi: 10.3390/ijms12095908.

[14] L. Uzun and A. P. F. Turner, "Molecularly-imprinted polymer sensors: realising their potential," *Biosens. Bioelectron.*, vol. 76, pp. 131–144, Feb. 2016, doi: 10.1016/j.bios.2015.07.013.

[15] S. A. Piletsky, Yu. P. Parhometz, N. V. Lavryk, T. L. Panasyuk, and A. V. El'skaya, "Sensors for low-weight organic molecules based on molecular imprinting technique," *Sens. Actuators B Chem.*, vol. 19, no. 1, pp. 629–631, Apr. 1994, doi: 10.1016/0925-4005(93)01216-Q.

[16] K. Mosbach, “Molecular imprinting,” *Trends Biochem. Sci.*, vol. 19, no. 1, pp. 9–14, Jan. 1994, doi: 10.1016/0968-0004(94)90166-X.
[17] J. Zhang, Q. Zhu, Y. Zhang, Z. Zhu, and Q. Liu, “Methanol Gas-Sensing Properties of SWCNT-MIP Composites,” *Nanoscale Res. Lett.*, vol. 11, no. 1, p. 522, Nov. 2016, doi: 10.1186/s11671-016-1675-3.
[18] L. Feng, Y. Liu, X. Zhou, and J. Hu, “The fabrication and characterization of a formaldehyde odor sensor using molecularly imprinted polymers,” *J. Colloid Interface Sci.*, vol. 284, no. 2, pp. 378–382, Apr. 2005, doi: 10.1016/j.jcis.2004.10.054.
[19] S. Haghdoust, U. Arshad, A. Mujahid, L. Schranzhofer, and P. A. Lieberzeit, “Development of a MIP-Based QCM Sensor for Selective Detection of Penicillins in Aqueous Media,” *Chemosensors*, vol. 9, no. 12, Art. no. 12, Dec. 2021, doi: 10.3390/chemosensors9120362.
[20] A. Jahangiri-Manesh, M. Mousazadeh, and M. Nikkhah, “Fabrication of chemiresistive nanosensor using molecularly imprinted polymers for acetone detection in gaseous state,” *Iran. Polym. J.*, vol. 31, no. 7, pp. 883–891, Jul. 2022, doi: 10.1007/s13726-022-01044-w.
[21] J. Völkle, K. Kumpf, A. Feldner, P. Lieberzeit, and P. Fruhmann, “Development of conductive molecularly imprinted polymers (cMIPs) for limonene to improve and interconnect QCM and chemiresistor sensing,” *Sens. Actuators B Chem.*, vol. 356, p. 131293, Apr. 2022, doi: 10.1016/j.snb.2021.131293.
[22] A. Raziq, A. Kidakova, R. Boroznjak, J. Reut, A. Öpik, and V. Syritski, “Development of a portable MIP-based electrochemical sensor for detection of SARS-CoV-2 antigen,” *Biosens. Bioelectron.*, vol. 178, p. 113029, Apr. 2021, doi: 10.1016/j.bios.2021.113029.
[23] M. Antipchik, J. Reut, A. G. Ayankojo, A. Öpik, and V. Syritski, “MIP-based electrochemical sensor for direct detection of hepatitis C virus via E2 envelope protein,” *Talanta*, vol. 250, p. 123737, Dec. 2022, doi: 10.1016/j.talanta.2022.123737.
[24] J. Feng *et al.*, “Highly sensitive and selective fluorescent sensor for tetrabromobisphenol-A in electronic waste samples using molecularly imprinted polymer coated quantum dots,” *Microchem. J.*, vol. 144, pp. 93–101, Jan. 2019, doi: 10.1016/j.microc.2018.08.041.
[25] R. Shariati, B. Rezaei, H. R. Jamei, and A. A. Ensafi, “Manufacturing of a Sensitive and Selective Optical Sensor Based on Molecularly Imprinted Polymers and Green Carbon Dots Synthesized from Cedrus Plant for Trace Analysis of Propranolol,” *Anal. Sci.*, vol. 35, no. 10, pp. 1083–1088, Oct. 2019, doi: 10.2116/analsci.19P133.
[26] C. H. Ashton, “Pharmacology and effects of cannabis: A brief review,” *Br. J. Psychiatry*, vol. 178, no. 2, pp. 101–106, Feb. 2001, doi: 10.1192/bjp.178.2.101.
[27] J. Sarris, J. Sinclair, D. Karamacoska, M. Davidson, and J. Firth, “Medicinal cannabis for psychiatric disorders: a clinically-focused systematic review,” *BMC Psychiatry*, vol. 20, no. 1, p. 24, Jan. 2020, doi: 10.1186/s12888-019-2409-8.
[28] M. A. ElSohly and W. Gul, “Constituents of Cannabis Sativa,” in *Handbook of Cannabis*, R. Pertwee, Ed., Oxford University Press, 2014, p. 0. doi: 10.1093/acprof:oso/9780199662685.003.0001.
[29] G. Lafaye, L. Karila, L. Blecha, and A. Benyamina, “Cannabis, cannabinoids, and health,” *Dialogues Clin. Neurosci.*, vol. 19, no. 3, pp. 309–316, Sep. 2017.
[30] J. M. McPartland and E. B. Russo, “Cannabis and Cannabis Extracts,” *J. Cannabis Ther.*, vol. 1, no. 3–4, pp. 103–132, Jun. 2001, doi: 10.1300/J175v01n03_08.
[31] L. Iversen, “Cannabis and the brain,” *Brain*, vol. 126, no. 6, pp. 1252–1270, Jun. 2003, doi: 10.1093/brain/awg143.

[32] H. Z. Khiabani and J. Mørland, "[Cannabis and cannabinoids as drugs]," *Tidsskr. Den Nor. Laegeforening Tidsskr. Prakt. Med. Ny Raekke*, vol. 127, no. 5, pp. 579–582, Mar. 2007.
[33] D. Baker, G. Pryce, G. Giovannoni, and A. J. Thompson, "The therapeutic potential of cannabis," *Lancet Neurol.*, vol. 2, no. 5, pp. 291–298, May 2003, doi: 10.1016/S1474-4422(03)00381-8.
[34] E. National Academies of Sciences, H. and M. Division, B. on P. H. and P. H. Practice, and C. on the H. E. of M. A. E. R. and R. Agenda, "Therapeutic Effects of Cannabis and Cannabinoids," in *The Health Effects of Cannabis and Cannabinoids: The Current State of Evidence and Recommendations for Research*, National Academies Press (US), 2017. Accessed: Jun. 12, 2023. [Online]. Available: https://www.ncbi.nlm.nih.gov/books/NBK425767/
[35] C. M. White, "A Review of Human Studies Assessing Cannabidiol's (CBD) Therapeutic Actions and Potential," *J. Clin. Pharmacol.*, vol. 59, no. 7, pp. 923–934, 2019, doi: 10.1002/jcph.1387.
[36] E. S. Seltzer, A. K. Watters, D. MacKenzie, L. M. Granat, and D. Zhang, "Cannabidiol (CBD) as a Promising Anti-Cancer Drug," *Cancers*, vol. 12, no. 11, Art. no. 11, Nov. 2020, doi: 10.3390/cancers12113203.
[37] S. Bonaccorso, A. Ricciardi, C. Zangani, S. Chiappini, and F. Schifano, "Cannabidiol (CBD) use in psychiatric disorders: A systematic review," *NeuroToxicology*, vol. 74, pp. 282–298, Sep. 2019, doi: 10.1016/j.neuro.2019.08.002.
[38] H. J. VanDolah, B. A. Bauer, and K. F. Mauck, "Clinicians' Guide to Cannabidiol and Hemp Oils," *Mayo Clin. Proc.*, vol. 94, no. 9, pp. 1840–1851, Sep. 2019, doi: 10.1016/j.mayocp.2019.01.003.
[39] P. Sharma, P. Murthy, and M. M. S. Bharath, "Chemistry, Metabolism, and Toxicology of Cannabis: Clinical Implications," *Iran. J. Psychiatry*, vol. 7, no. 4, pp. 149–156, 2012.
[40] K. Amini, A. Sepehrifard, A. Valinasabpouri, J. Safruk, D. Angelone, and T. de Campos Lourenco, "Recent advances in electrochemical sensor technologies for THC detection—a narrative review," *J. Cannabis Res.*, vol. 4, no. 1, p. 12, Mar. 2022, doi: 10.1186/s42238-022-00122-3.
[41] V. Ramzy and R. Priefer, "THC detection in the breath," *Talanta*, vol. 222, p. 121528, Jan. 2021, doi: 10.1016/j.talanta.2020.121528.
[42] T. R. Arkell *et al.*, "Detection of Δ9 THC in oral fluid following vaporized cannabis with varied cannabidiol (CBD) content: An evaluation of two point-of-collection testing devices," *Drug Test. Anal.*, vol. 11, no. 10, pp. 1486–1497, 2019, doi: 10.1002/dta.2687.
[43] S. Prashad and F. M. Filbey, "Cognitive motor deficits in cannabis users," *Curr. Opin. Behav. Sci.*, vol. 13, pp. 1–7, Feb. 2017, doi: 10.1016/j.cobeha.2016.07.001.
[44] N. D. Volkow, R. D. Baler, W. M. Compton, and S. R. B. Weiss, "Adverse Health Effects of Marijuana Use," *N. Engl. J. Med.*, vol. 370, no. 23, pp. 2219–2227, Jun. 2014, doi: 10.1056/NEJMra1402309.
[45] C. Burnier, P. Esseiva, and C. Roussel, "Quantification of THC in Cannabis plants by fast-HPLC-DAD: A promising method for routine analyses," *Talanta*, vol. 192, pp. 135–141, Jan. 2019, doi: 10.1016/j.talanta.2018.09.012.
[46] P. S. Tzimas, E. A. Petrakis, M. Halabalaki, and L. A. Skaltsounis, "Effective determination of the principal non-psychoactive cannabinoids in fiber-type Cannabis sativa L. by UPLC-PDA following a comprehensive design and optimization of extraction

methodology," *Anal. Chim. Acta*, vol. 1150, p. 338200, Mar. 2021, doi: 10.1016/j.aca.2021.338200.
[47] C. Citti, D. Braghiroli, M. A. Vandelli, and G. Cannazza, "Pharmaceutical and biomedical analysis of cannabinoids: A critical review," *J. Pharm. Biomed. Anal.*, vol. 147, pp. 565–579, Jan. 2018, doi: 10.1016/j.jpba.2017.06.003.
[48] B. Nie, J. Henion, and I. Ryona, "The Role of Mass Spectrometry in the Cannabis Industry," *J. Am. Soc. Mass Spectrom.*, vol. 30, no. 5, pp. 719–730, May 2019, doi: 10.1007/s13361-019-02164-z.
[49] S. Porcu *et al.*, "Rapid In Situ Detection of THC and CBD in Cannabis sativa L. by 1064 nm Raman Spectroscopy," *Anal. Chem.*, vol. 94, no. 29, pp. 10435–10442, Jul. 2022, doi: 10.1021/acs.analchem.2c01629.
[50] R. K. Mishra *et al.*, "Simultaneous detection of salivary Δ9-tetrahydrocannabinol and alcohol using a Wearable Electrochemical Ring Sensor," *Talanta*, vol. 211, p. 120757, May 2020, doi: 10.1016/j.talanta.2020.120757.
[51] Q. Zhang, D. Berg, and S. M. Mugo, "Molecularly imprinted carbon based electrodes for tetrahydrocannabinol sensing," *Inorg. Chem. Commun.*, vol. 107, p. 107459, Sep. 2019, doi: 10.1016/j.inoche.2019.107459.
[52] C. Wanklyn *et al.*, "Disposable screen printed sensor for the electrochemical detection of delta-9-tetrahydrocannabinol in undiluted saliva," *Chem. Cent. J.*, vol. 10, no. 1, p. 1, Jan. 2016, doi: 10.1186/s13065-016-0148-1.
[53] K. Solin, M. Vuoriluoto, A. Khakalo, and T. Tammelin, "Cannabis detection with solid sensors and paper-based immunoassays by conjugating antibodies to nanocellulose," *Carbohydr. Polym.*, vol. 304, p. 120517, Mar. 2023, doi: 10.1016/j.carbpol.2022.120517.
[54] S. Yüksel *et al.*, "Trace detection of tetrahydrocannabinol (THC) with a SERS-based capillary platform prepared by the in situ microwave synthesis of AgNPs," *Anal. Chim. Acta*, vol. 939, pp. 93–100, Oct. 2016, doi: 10.1016/j.aca.2016.08.033.
[55] K. Sivashanmugan *et al.*, "Trace Detection of Tetrahydrocannabinol in Body Fluid via Surface-Enhanced Raman Scattering and Principal Component Analysis," *ACS Sens.*, vol. 4, no. 4, pp. 1109–1117, Apr. 2019, doi: 10.1021/acssensors.9b00476.
[56] K. Sivashanmugan, Y. Zhao, and A. X. Wang, "Tetrahydrocannabinol Sensing in Complex Biofluid with Portable Raman Spectrometer Using Diatomaceous SERS Substrates," *Biosensors*, vol. 9, no. 4, Art. no. 4, Dec. 2019, doi: 10.3390/bios9040125.
[57] A. Kudelski, "Analytical applications of Raman spectroscopy," *Talanta*, vol. 76, no. 1, pp. 1–8, Jun. 2008, doi: 10.1016/j.talanta.2008.02.042.
[58] J. Guo, Y. Liu, H. Ju, and G. Lu, "From lab to field: Surface-enhanced Raman scattering-based sensing strategies for on-site analysis," *TrAC Trends Anal. Chem.*, vol. 146, p. 116488, Jan. 2022, doi: 10.1016/j.trac.2021.116488.
[59] R. L. McCreery, *Raman Spectroscopy for Chemical Analysis*. John Wiley & Sons, 2005.
[60] J. R. Ferraro, *Introductory Raman Spectroscopy*. Elsevier, 2003.
[61] I. R. Lewis and H. G. M. Edwards, *Handbook of Raman spectroscopy: from the research laboratory to the process line*. in Practical spectroscopy. New York: Marcel Dekker, 2001. Accessed: Jun. 17, 2023. [Online]. Available: http://www.crcnetbase.com/isbn/9781420029253
[62] "Guide to Raman Spectroscopy." https://www.bruker.com/en/products-and-solutions/infrared-and-raman/raman-spectrometers/what-is-raman-spectroscopy.html (accessed Jun. 17, 2023).

[63] D. J. Gardiner and P. R. Graves, Eds., *Practical Raman Spectroscopy*. Berlin, Heidelberg: Springer, 1989. doi: 10.1007/978-3-642-74040-4.
[64] K. Kneipp, H. Kneipp, I. Itzkan, R. R. Dasari, and M. S. Feld, "Ultrasensitive Chemical Analysis by Raman Spectroscopy," *Chem. Rev.*, vol. 99, no. 10, pp. 2957–2976, Oct. 1999, doi: 10.1021/cr980133r.
[65] X. Yang, A. S. P. Chang, B. Chen, C. Gu, and T. C. Bond, "High sensitivity gas sensing by Raman spectroscopy in photonic crystal fiber," *Sens. Actuators B Chem.*, vol. 176, pp. 64–68, Jan. 2013, doi: 10.1016/j.snb.2012.09.004.
[66] A. Orlando *et al.*, "A Comprehensive Review on Raman Spectroscopy Applications," *Chemosensors*, vol. 9, no. 9, Art. no. 9, Sep. 2021, doi: 10.3390/chemosensors9090262.
[67] C. Lin *et al.*, "Recent development of surface-enhanced Raman scattering for biosensing," *J. Nanobiotechnology*, vol. 21, no. 1, p. 149, May 2023, doi: 10.1186/s12951-023-01890-7.
[68] P. L. Stiles, J. A. Dieringer, N. C. Shah, and R. P. Van Duyne, "Surface-Enhanced Raman Spectroscopy," *Annu. Rev. Anal. Chem.*, vol. 1, no. 1, pp. 601–626, Jul. 2008, doi: 10.1146/annurev.anchem.1.031207.112814.
[69] "Surface-Enhanced Raman Scattering and Surface-Enhanced Resonance Raman Scattering," in *Modern Raman Spectroscopy – A Practical Approach*, John Wiley & Sons, Ltd, 2004, pp. 113–133. doi: 10.1002/0470011831.ch5.
[70] J. Guo *et al.*, "High-Sensitivity Raman Gas Probe for In Situ Multi-Component Gas Detection," *Sensors*, vol. 21, no. 10, Art. no. 10, Jan. 2021, doi: 10.3390/s21103539.
[71] W. Wang, P. Ma, and D. Song, "Applications of surface-enhanced Raman spectroscopy based on portable Raman spectrometers: A review of recent developments," *Luminescence*, vol. 37, no. 11, pp. 1822–1835, 2022, doi: 10.1002/bio.4383.
[72] J. Sun, L. Gong, W. Wang, Z. Gong, D. Wang, and M. Fan, "Surface-enhanced Raman spectroscopy for on-site analysis: A review of recent developments," *Luminescence*, vol. 35, no. 6, pp. 808–820, 2020, doi: 10.1002/bio.3796.
[73] J. Ma *et al.*, "An overview on molecular imprinted polymers combined with surface-enhanced Raman spectroscopy chemical sensors toward analytical applications," *Talanta*, vol. 225, p. 122031, Apr. 2021, doi: 10.1016/j.talanta.2020.122031.
[74] X. Ren, E. C. Cheshari, J. Qi, and X. Li, "Silver microspheres coated with a molecularly imprinted polymer as a SERS substrate for sensitive detection of bisphenol A," *Microchim. Acta*, vol. 185, no. 4, p. 242, Apr. 2018, doi: 10.1007/s00604-018-2772-z.
[75] Y. Lv, Y. Qin, F. Svec, and T. Tan, "Molecularly imprinted plasmonic nanosensor for selective SERS detection of protein biomarkers," *Biosens. Bioelectron.*, vol. 80, pp. 433–441, Jun. 2016, doi: 10.1016/j.bios.2016.01.092.
[76] M. Bompart, Y. De Wilde, and K. Haupt, "Chemical Nanosensors Based on Composite Molecularly Imprinted Polymer Particles and Surface-Enhanced Raman Scattering," *Adv. Mater.*, vol. 22, no. 21, pp. 2343–2348, 2010, doi: 10.1002/adma.200904442.
[77] S. Araki, M. Watanabe, F. Sassa, and K. Hayashi, "Raman enhanced structure with reconfigured molecularly-imprinted-polymer for gas deteciton," in *2016 IEEE SENSORS*, Oct. 2016, pp. 1–3. doi: 10.1109/ICSENS.2016.7808604.
[78] Y. Kou *et al.*, "Recyclable Magnetic MIP-Based SERS Sensors for Selective, Sensitive, and Reliable Detection of Paclobutrazol Residues in Complex Environments," *ACS Sustain. Chem. Eng.*, vol. 8, no. 38, pp. 14549–14556, Sep. 2020, doi: 10.1021/acssuschemeng.0c05065.

[79] E. Ekmen, M. Bilici, E. Turan, U. Tamer, and A. Zengin, “Surface molecularly-imprinted magnetic nanoparticles coupled with SERS sensing platform for selective detection of malachite green,” *Sens. Actuators B Chem.*, vol. 325, p. 128787, Dec. 2020, doi: 10.1016/j.snb.2020.128787.
[80] R. Schmitt, “Scanning Electron Microscope,” in *CIRP Encyclopedia of Production Engineering*, L. Laperrière and G. Reinhart, Eds., Berlin, Heidelberg: Springer, 2014, pp. 1085–1089. doi: 10.1007/978-3-642-20617-7_6595.
[81] K. D. Vernon-Parry, “Scanning electron microscopy: an introduction,” *III-Vs Rev.*, vol. 13, no. 4, pp. 40–44, Jul. 2000, doi: 10.1016/S0961-1290(00)80006-X.
[82] S. P. Mulvaney and C. D. Keating, “Raman Spectroscopy,” *Anal. Chem.*, vol. 72, no. 12, pp. 145–158, Jun. 2000, doi: 10.1021/a10000155.
[83] P. Rostron and D. Gerber, “Raman Spectroscopy, a review,” *Int. J. Eng. Tech. Res.*, vol. 6, pp. 50–64, Sep. 2016.
[84] M. M. El-Beshlawy, F. M. Abdel-Haleem, A. H. Kamel, and A. Barhoum, “Screen-Printed Sensors Coated with Polyaniline/Molecularly Imprinted Polymer Membranes for the Potentiometric Determination of 2,4-Dichlorophenoxyacetic Acid Herbicide in Wastewater and Agricultural Soil,” *Chemosensors*, vol. 11, no. 1, Art. no. 1, Jan. 2023, doi: 10.3390/chemosensors11010003.
[85] S. Janfaza *et al.*, “A Nanostructured Microfluidic Artificial Olfaction for Organic Vapors Recognition,” *Sci. Rep.*, vol. 9, no. 1, p. 19051, Dec. 2019, doi: 10.1038/s41598-019-55672-z.
[86] S. Janfaza, M. Banan Nojavani, M. Nikkhah, T. Alizadeh, A. Esfandiar, and M. R. Ganjali, “A selective chemiresistive sensor for the cancer-related volatile organic compound hexanal by using molecularly imprinted polymers and multiwalled carbon nanotubes,” *Microchim. Acta*, vol. 186, no. 3, p. 137, Feb. 2019, doi: 10.1007/s00604-019-3241-z.
[87] T. Kamra *et al.*, “Photoconjugation of Molecularly Imprinted Polymer Nanoparticles for Surface-Enhanced Raman Detection of Propranolol,” *ACS Appl. Mater. Interfaces*, vol. 7, no. 49, pp. 27479–27485, Dec. 2015, doi: 10.1021/acsami.5b09500.
[88] K. Kantarovich, A.-S. Belmont, K. Haupt, I. Bar, and L. A. Gheber, “Detection of template binding to molecularly imprinted polymers by Raman microspectroscopy,” *Appl. Phys. Lett.*, vol. 94, no. 19, p. 194103, May 2009, doi: 10.1063/1.3132061.
[89] S. K. Islam, Y. P. Cheng, R. L. Birke, M. V. Cañamares, C. Muehlethaler, and J. R. Lombardi, “An analysis of tetrahydrocannabinol (THC) and its analogs using surface enhanced Raman Scattering (SERS),” *Chem. Phys.*, vol. 536, p. 110812, Aug. 2020, doi: 10.1016/j.chemphys.2020.110812.
[90] Z. Wang, H. Li, X. Wang, J. Jiang, H. Sun, and L. Wang, “Determination of 2,6-Dichlorophenol by Surface-Enhanced Raman Scattering with Molecular Imprinting,” *Anal. Lett.*, vol. 51, no. 13, pp. 2062–2072, Sep. 2018, doi: 10.1080/00032719.2017.1399414.